Runx2 regulates mouse tooth root development via activation of WNT inhibitor *Notum*

Quan Wen[1,2], Junjun Jing[1], Xia Han[1], Jifan Feng[1], Yuan Yuan[1], Yuanyuan Ma[1], Shuo Chen[1], Thach-Vu Ho[1], and Yang Chai[1,*]

[1]Center for Craniofacial Molecular Biology, University of Southern California, Los Angeles, CA 90033, USA.
[2]Peking University Hospital of Stomatology First Clinical Division, 37A Xishiku Street, Xicheng District, Beijing, 100034, China.

*Corresponding author:
Yang Chai
Center for Craniofacial Molecular Biology
University of Southern California
2250 Alcazar Street – CSA 103
Los Angeles, CA 90033
Phone number: 323-442-3480
ychai@usc.edu

Short title: *Runx2* regulates root development via *Notum*

Abstract

Progenitor cells are crucial in controlling organ morphogenesis. Tooth development is a well-established model for investigating the molecular and cellular mechanisms that regulate organogenesis. Despite advances in our understanding of how tooth crown formation is regulated, we have limited understanding of tooth root development. RUNX2 is a well-known transcription factor in osteogenic differentiation and early tooth development. However, the function of RUNX2 during tooth root formation remains unknown. We revealed in this study that RUNX2 is expressed in a subpopulation of GLI1+ root progenitor cells, and that loss of *Runx2* in these GLI1+ progenitor cells and their progeny results in root developmental defects. Our results provide *in vivo* evidence that *Runx2* plays a crucial role in tooth root development and in regulating the differentiation of root progenitor cells. Furthermore, we identified that *Gli1*, *Pcp4*, *Notum*, and *Sfrp2* are downstream targets of *Runx2* by integrating bulk and single-cell RNA sequencing analyses. Specifically, ablation of *Runx2* results in downregulation of WNT inhibitor *Notum* and upregulation of canonical WNT signaling in the odontoblastic site, which disturbs normal odontoblastic differentiation. Significantly, exogenous NOTUM partially rescues the impaired root development in *Runx2* mutant molars. Collectively, our studies elucidate how *Runx2* achieves functional specificity in regulating the development of diverse organs and yields new insights into the network that regulates tooth root development.

Key words: *Runx2*, *Gli1*, *Notum*, WNT/β-catenin, root development

Introduction

Teeth perform extensive functions in our daily lives, not only by participating in crucial physiological processes such as mastication, but also by contributing significantly to the aesthetics of the craniofacial complex. Teeth are composed of two major parts, the crown and the root. The crown is the visible component in the oral cavity, while the root extends into the jawbone and integrates our dentition with mandible and maxilla. Similar to how most ectodermal organs develop, tooth morphogenesis involves sequence of reciprocal inductive molecular interactions between dental epithelium and underlying cranial neural crest-derived ectomesenchymal cells.[1,2]

It has long been recognized that the tooth provides an excellent model for studying the regulation of organogenesis. The regulatory network that governs tooth crown development has been extensively studied,[3-5] but the regulatory mechanism of root development remains largely unknown. Studies have shown that major signaling pathways, such as TGF-β, BMP, FGF, WNT, SHH and PTHrP/PTH1R participate in root development,[6,7] but it is not yet known how these signals achieve their functional specificity in root development. It is plausible that a network of transcription factors may play a crucial role in this process.[8]

The transcription factor RUNX2 is well known for its regulatory role in osteogenesis and tooth development. It is indispensable for mesenchymal progenitor cells' commitment to the osteoblastic lineage and also modulates their proliferation, differentiation, and maintenance.[9] In humans, *RUNX2* mutations can cause an autosomal dominant syndrome, cleidocranial dysplasia (CCD), which affects the bones and teeth and is characterized by short stature, delayed cranial suture closure, abnormal clavicle formation, and dental anomalies, including delayed tooth eruption and supernumerary teeth.[10] The dental anomalies in CCD patients suggest the importance of RUNX2 in tooth formation and eruption, but no root defect has been reported in these patients. Several

studies using animal models have revealed that *Runx2* is required for early tooth development. *Runx2*-deficient mice exhibit arrested molar and incisor development at the early cap stage.[11] Ablation of *Runx2* in dental epithelium using *K14-cre* suppresses enamel maturation.[12] Together, these studies lead to the conclusion that *Runx2* is essential for normal crown formation. However, to date, it remains unknown whether and how *Runx2* regulates tooth root development.

Previously, we have identified that GLI1+ cells are progenitor cells in mouse molar root development: they show classic mesenchymal stem cell (MSC) characteristics *in vitro* and support root formation *in vivo*.[8] To test the functional significance of *Runx2* in the regulation of tooth root development, we first analyzed RUNX2 expression during root development. Our data show that RUNX2 is expressed in a subpopulation of GLI1+ cells and that loss of *Runx2* in these GLI1+ cells results in root developmental defects. Furthermore, we identified several *Runx2* downstream target genes, shedding light on the molecular regulatory mechanism that controls tooth root development. Notably, we found that *Runx2* is required for WNT inhibitor *Notum* expression and regulates canonical WNT signaling to activate the odontoblastic lineage commitment of root progenitor cells during root development. This discovery highlights the specific signaling mechanism by which *Runx2* may exert its regulatory role during tooth root development.

Material and Methods

Animal Information

Mice used in this study included *Gli1-Cre*^{ERT2} knock-in (JAX#007913, The Jackson Laboratory),[13] *tdTomato* conditional reporter (JAX#007905, The Jackson Laboratory),[14] conditional *Runx2* floxed (a gift from Dr. Yukio Yoneda, Kanazawa, Japan),[15] *Gli1-LacZ* knock-in/knock-out reporter (JAX#008211, The Jackson Laboratory),[16] *Runx2-rtTA* (a gift from Dr. Fanxin Long, Washington University, St. Louis, USA),[17] *tetO-Cre* (JAX#006234, The Jackson Laboratory),[18] and *Dmp1-Cre*.[19] Mice were housed in pathogen-free conditions in the animal facility of the University of Southern California. Mice were used for analysis irrespective of sex. Ear tissue was collected and lysed in DirectPCR reagent (Viagen, #102-T) with Proteinase K (Viagen, #501-PK) at 85°C for 1 hour, followed by PCR-based genotyping. All the animal studies followed protocols approved by the Department of Animal Resources and the Institutional Animal Care and Use Committee of the University of Southern California.

Tamoxifen and Doxycycline Administration

Tamoxifen (Sigma T5648) was dissolved in corn oil (Sigma C8267) at 20 mg/ml and injected intraperitoneally once at postnatal day 3.5 (PN3.5) at a dose of 1.5mg/10g body weight. Doxycycline rodent diet (Envigo, TD.08541) was administered every day from PN3.5 to PN7.5; meanwhile, doxycycline (Sigma D9891) was dissolved in NS at 5 mg/ml and injected intraperitoneally at PN3.5 and PN5.5 at a dose of 50 μg/g of body weight.

Histological Analysis

Dissected mandibles were fixed in 4% paraformaldehyde for 24h and then decalcified in 10% EDTA (pH 7.4) for 1-4 weeks, depending on the age of the mice. For paraffin sectioning,

decalcified samples were dehydrated in Spin Tissue Processor, then embedded in paraffin and sectioned at 5 μm using a microtome (Leica RM2255). Hematoxylin and Eosin (H&E) staining was performed using standard procedures. For frozen sectioning, decalcified samples were dehydrated in 15% sucrose/PBS solution followed by 30% sucrose/PBS solution, then embedded in OCT compound (Tissue-Tek, Sakura) and cryosectioned at 8 μm using a cryostat (Leica CM3050S). All the images were captured by an All-in-one Fluorescence Microscope (Keyence, BZ-X710).

Immunostaining

Frozen sections were washed in PBST, blocked with TNB Blocking Buffer (PerkinElmer FP1020) for 1h, and incubated with primary antibody at 4℃ overnight. After washing in PBST, sections were incubated with Alexa-conjugated secondary antibody for 1h at RT. DAPI (Abcam, ab104139) was used for nuclear staining.

Antibodies used in our study were: RUNX2 (Cell Signaling, 12556S, 1:200), β-Galactosidase (Abcam, ab9361, 1:500), Ki67 (Abcam, ab15580, 1:500), Goat anti-Rabbit IgG Alexa Fluor 488/568 (Invitrogen, A11034, A11011, 1:200), and Goat anti-chicken IgY Alexa Fluor 568 (Invitrogen, A11041, 1:200).

RNAscope *in situ* hybridization

RNAscope 2.5 HD Reagent Kit-RED (Advanced Cell Diagnostics, 322350) and RNAscope Multiplex Fluorescent v2 (Advanced Cell Diagnostics, 323110) were used in our study to detect gene expression *in situ* on frozen sections, according to the manufacturer's instructions. All the probes were purchased from Advanced Cell Diagnostics, including Dspp (448301), Gli1 (311001),

Pcp4 (402311), Sfrp2 (400381), Notum (428981), Axin2 (400331), Wnt3a (405041), and Wnt4 (401101).

MicroCT analysis

Fixed samples were scanned using a SCANCO μCT50 (Scanno V1.28) at the University of Southern California Molecular Imaging Center. The microCT images were captured at a resolution of 10 μm under an x-ray source of 90 kVp and 78μA. Three-dimensional reconstruction was done using AVIZO 9.5 (Visualization Sciences Group).

Quantitative RT-PCR

Mandibular first molars of PN7.5 or PN21.5 mice were carefully dissected on ice. Four mice were used for each group. The apical half of each molar was used for RNA extraction using RNeasy Plus Micro Kit (Qiagen, 74034). Quantitative RT-PCR analysis was performed using iScript cDNA Synthesis kit (Bio-Rad), SsoFast EvaGreen Supermix (Bio-Rad) and Bio-Rad CFX96 Real-Time Systems. Data analysis was following the $2^{-\Delta\Delta CT}$ method. The primer sequences were obtained from PrimerBank and are listed in Supplemental Table 1.[20]

ChIP assay

ChIP assay was performed using the apical halves of mandibular first molars of control PN7.5 mice, and tissues from approximately 20 mice were combined to comprise one sample. Chromatrap ChIP kit (500191) was used in our experiment. After immunoprecipitation with anti-RUNX2 antibody (Cell Signaling, 12556S), or rabbit IgG (Chromatrap), real-time qPCR was performed using the primers in Supplemental Table 1.

Bulk RNA Sequencing Analysis

Gli1-Cre^{ERT2};Runx2$^{fl/fl}$ and *Runx2$^{fl/fl}$* littermate control mice received injection of tamoxifen at PN3.5 and were euthanized 4 days later. The apical halves of the mandibular first molars were dissected for RNA extraction. Each sample contained tissue from 4 mice. cDNA library preparation and sequencing were carried out by the Technology Center for Genomics & Bioinformatics at the University of California, Los Angeles (UCLA). A total of 200 million pair-end reads were obtained on NovaSeq 6000 S2 for 4 pairs of samples. The raw data was analyzed using Partek® Flow® software. Briefly, raw reads were trimmed, aligned by STAR (2.6.1d) with the mm10 genome, and normalized using FPKM. Differential analysis was performed using the gene set analysis (GSA) method. P-value < 0.05 and fold change < -1.8 or > 1.8 across groups were considered significant.

Single-Cell RNA Sequencing Analysis

Isolation of cells and sequencing

Gli1-Cre^{ERT2};Runx2$^{fl/fl}$ and *Runx2$^{fl/fl}$* littermate control mice were injected with tamoxifen at PN3.5 and euthanized 4 days later. Whole mandibular first molars were collected in PBS on ice, with each sample containing 8 molars total from 4 mice. Then the molars were cut into small pieces and transferred into digestion solution (2 mg/ml Collagenase I + 2 mg/ml Dispase, dissolved in HBSS). Samples were incubated at 37℃ with rotation in a Hybaid Oven for 25 minutes, with occasional pipetting. Then the samples were passed through a Flowmi® cell strainer (Scienceware®, porosity 40 μm) to obtain a single-cell suspension. The Chromium Single Cell 3' Reagent Kits v3 was used for GEM generation and library construction, according to the protocols provided by the manufacturer. The cDNA sequencing was conducted by the Technology Center for Genomics & Bioinformatics at UCLA. Quality control, mapping, and count table assembly of the library were performed using the CellRanger pipeline version 3.1.0.

Integration analysis of control and mutant samples

Raw read counts from the control and *Gli1-Cre^{ERT2};Runx2$^{fl/fl}$* sample were analyzed using the Seurat v3 R package.[21,22] Data were first filtered and normalized, then the FindVariableGenes function was used to select variable genes. The FindIntegrationAnchors function was used to identify "anchors" across the two datasets, which were then used to integrate the two datasets with the IntegrateData function. Scaledata, Principal Component Analysis (PCA) and UMAP visualization were then performed for downstream analysis and visualization.

Assay for Transposase Accessible Chromatin sequencing (ATAC-seq) Analysis

The ATAC-seq analysis was performed following standard protocols.[23] Briefly, the apical halves of 8 mandibular first molars of PN7.5 *Runx2$^{fl/fl}$* control mice were collected in PBS on ice. Then the tissues were treated with the same method described in our scRNA-seq to obtain a single-cell suspension. 50,000 cells were lysed, and followed by transposition reaction and purification, and PCR amplification. The library construction and sequencing were performed by the Molecular Genomics Core at the University of Southern California, Los Angeles (USC). The raw data was analyzed using Partek® Flow® software. Briefly, raw reads were aligned using Bowtie2 with the mm10 genome; MACS2 was used for detecting genomic enrichment regions; RUNX2 binding motifs were analyzed using HOMER.[24] Output files were uploaded to the UCSC genome browser for visualization.

Cell culture and odontoblastic differentiation

Dental pulp tissue from the mandibular first molars of 10 PN7.5 mice was obtained, minced into small pieces, and seeded on a 6 cm cell culture dish (Corning) with α-MEM + 10% FBS (GIBCO) at 37℃ in a 5% CO_2 incubator. When the primary cells reached 80% confluent, the cells were

passed for odontoblastic differentiation. The odontoblastic differentiation medium contained 1% FBS, 5 mM β-glycerophosphate (Sigma, G9422), 50 μg/ml ascorbic acid (Sigma, A4403) and 10^{-7} M dexamethasone (Sigma, D4902).[25]

Kidney capsule transplantation

Gli1-Cre^{ERT2};Runx2$^{fl/fl}$ and *Runx2$^{fl/fl}$* littermate control mice were injected with tamoxifen at PN3.5 and euthanized 2 days later. Whole mandibular first molars were carefully dissected and placed in PBS on ice. Host mice were anesthetized using isoflurane, then fur on the back was shaved and the kidney on the left side was exposed through a skin incision. The kidney capsule was opened using fine-tip forceps. Two explants were transplanted under the kidney capsule of one host. Three weeks later, the explants were harvested for histological analysis. For the rescue experiment, Affi-Gel blue agarose beads (Bio-Rad, 1537301) were wash in PBS and then incubated in recombinant mouse Notum protein (100 μg/ml, R&D systems, 9150-NO) or bovine serum albumin (BSA) (100 μg/mL) for 1 hour at 37℃ before transplantation. Notum beads or BSA beads were then applied to the explants from *Gli1-Cre^{ERT2};Runx2$^{fl/fl}$* mice and transplanted under the kidney capsule.

Statistical Analysis

GraphPad Prism 8 and Microsoft Office 2016 were used for statistical analysis. Results are represented as boxplots showing each data point, the median and the interquartile range. Significance was assessed by independent two-tailed Student's t tests. $P < 0.05$ was considered statistically significant. $N \geq 3$ for sample size; all experiments were repeated in triplicate or more to confirm the results unless otherwise stated.

Results

RUNX2 expression overlaps with a subpopulation of Gli1+ cells during root development

RUNX2 is expressed throughout tooth crown development which occurs mainly at embryonic stages in mice.[26] Shortly after tooth development initiates, RUNX2 expression is already detectable in the odontogenic mesenchyme, and remains strong during the bud and cap stages, but is downregulated at the bell and postnatal stages.[11] To determine whether *Runx2* is associated with root development, we examined the expression pattern of RUNX2 at different stages of root development and compared the pattern to that of GLI1+ cells and their progeny. At PN3.5, prior to root formation, RUNX2 is expressed in the apical dental papilla, dental follicle and surrounding bones, and its expression overlaps with a subset of the GLI1+ cells in the apical region of the dental mesenchyme (Fig. 1A-D). We also performed lineage tracing of GLI1+ cells to label their progeny from PN3.5. Four days later, upon the initiation of root formation, GLI1+ cells were present in the root-forming apical mesenchyme and dental epithelium, while RUNX2 expression colocalized with them in a more restricted area around Hertwig's epithelial root sheath (HERS), an epithelial structure that guides root formation, as well as in the preodontoblast region (Fig. 1E-H). At PN21.5, when root development is complete, progeny of these GLI1+ cells contributed to the entire root structure, including odontoblasts, pulp cells, periodontal ligament, alveolar bone, and the remaining dental epithelium; they colocalized with RUNX2 in the periodontal ligament, alveolar bone, and some odontoblasts (Fig. 1I-L, S2A-C). These results suggest RUNX2 expression overlaps with a subpopulation of GLI1+ cells during root development, and RUNX2 may be essential for GLI1+ progenitor cells to differentiate into odontoblasts and other root structures.

To test whether RUNX2+ cells are progenitor cells, we analyzed their contribution to the dental mesenchyme during tooth root development. RUNX2+ cells in *Runx2-rtTA;Teto-Cre;Tdt*$^{fl/+}$ mice

were labelled by doxycycline administration from PN3.5 to PN7.5. After labeling at PN7.5, we located RUNX2+ cells (tdTomato+) in the most apical region of the dental papilla, in the dental follicle and in odontoblasts (Fig. S1A, B). Eighteen days later, only a few odontoblasts and pulp cells were labeled (Fig. S1C, D), indicating that RUNX2+ cells do not contribute to root growth, and therefore are not root progenitor cells. As a technical matter, we note that *Runx2-rtTA* is a BAC transgenic line with the cDNA for rtTA2^{S}-M2 replacing the first exon of the *Runx2* gene. Previously published work suggests that *Runx2-rtTA* targets osteoblast-lineage cells.[17] RUNX2 has two major N-terminal isoforms: RUNX2-I is encoded by exons 2-8, while RUNX2-II is encoded by exons 1-8, which means *Runx2-rtTA* may only target the RUNX2-II-expressing cells.

Loss of *Runx2* results in tooth root development defects

Although *Runx2* have limited contribution to the root growth, RUNX2+ cells are located in the region of GLI1+ progenitor cells. To test the significance of *Runx2*'s function for tooth root development, we generated *Gli1-Cre^{ERT2};Runx2$^{fl/fl}$* mice and administered tamoxifen at PN3.5 to specifically delete *Runx2* in GLI1+ root progenitor cells and their progeny before the initiation of root formation. We confirmed that *Runx2* was efficiently deleted by tamoxifen induction, with no RUNX2 expression detectable in the dental mesenchyme of *Gli1-Cre^{ERT2};Runx2$^{fl/fl}$* mice (Fig. S2A-F). Ablation of *Runx2* resulted in severe root development defects (Fig. 2A-J). At PN21.5, the molar roots in control mice were well developed and had erupted, and the odontoblasts, pulp cells, periodontal ligament, and alveolar bone were properly formed (Fig. 2A, B, E-G). In contrast, the roots in *Gli1-Cre^{ERT2};Runx2$^{fl/fl}$* mice were much shorter and the teeth had not yet erupted, although the crowns appeared to be normal (Fig. 2C, D, H, S2G). In addition, the root dentin was much thinner, and the root odontoblasts lost their columnar structure, while the nuclei were not polarized (Fig. 2H-J). Consistent with impaired odontoblast differentiation, the expression of

dentin sialophophoprotein (*Dspp*), a marker of odontoblast differentiation, was absent in the root region (Fig. 2K, N, S2H), suggesting *Runx2* is required for the odontoblastic lineage commitment of GLI1+ root progenitor cells. The formation of the periodontal ligament, cementoblasts, and alveolar bone was also deficient in *Gli1-Cre^{ERT2};Runx2$^{fl/fl}$* mice (Fig. 2H-J). Moreover, we found that there were more proliferating cells in the apical dental mesenchyme around HERS (Fig. 2L, M, O, P, S2I), probably due to these cells failing to differentiate in *Gli1-Cre^{ERT2};Runx2$^{fl/fl}$* mice. This was further confirmed by lineage tracing of GLI1+ cells after deletion of *Runx2* in *Gli1-Cre^{ERT2};Runx2$^{fl/fl}$;tdTomato$^{fl/+}$* mice. The progeny of GLI1+ cells remained in the apical area, failing to contribute to root elongation and the formation of periodontium and alveolar bone as observed in control mice (Fig. S2A-F).

The *Gli1-Cre^{ERT2};Runx2$^{fl/fl}$* mice also developed a severe CCD-like phenotype, characterized by smaller body size and impaired skeletal development, including delayed cranial suture closure, hypoplastic clavicles, and micrognathia (Fig. S3A-I). Heterozygous mutation of *RUNX2* in humans and mice can cause CCD,[10,27] but we failed to detect any bone formation defects (data not shown) or root formation defects in *Gli1-Cre^{ERT2};Runx2$^{fl/+}$* mice (Fig. S4D-F). These results may indicate that *Runx2* also plays an important role at earlier stages in GLI1+ cells, and/or that it is important in GLI1- cells as well as in GLI1+ cells. Since *Runx2* is also expressed in mature odontoblasts, to investigate whether loss of *Runx2* in these cells has an effect on root development, we generated *Dmp1-Cre;Runx2$^{fl/fl}$* mice but did not identify any obvious defect in dentinogenesis (Fig. S4G-I), suggesting that loss of *Runx2* in mature odontoblasts does not affect odontoblast differentiation or root elongation. Taken together, our studies suggest that *Runx2* is indispensable for the differentiation of GLI1+ root progenitor cells to support root formation.

Identification of *Runx2* downstream target genes during root development

In order to identify downstream targets of *Runx2* that may regulate GLI1+ MSC differentiation, we collected the apical halves of molars at PN7.5-four days after Tamoxifen induction from both control and *Gli1-Cre^{ERT2};Runx2$^{fl/fl}$* mice for bulk RNA sequencing. In total, 427 genes were differentially expressed between these two groups, among them 219 upregulated and 208 downregulated in *Gli1-Cre^{ERT2};Runx2$^{fl/fl}$* mice, and the heatmap displays a distinct separation between the groups (Fig. 3A).

To map the differentially expressed genes back to their anatomic location at single-cell resolution, we conducted single-cell RNA sequencing (scRNA-seq) of whole PN7.5 molars from control and *Gli1-Cre^{ERT2};Runx2$^{fl/fl}$* mice to distinguish the expression patterns of these differentially expressed genes. A total of 4394 cells from control mice and 4764 cells from *Gli1-Cre^{ERT2};Runx2$^{fl/fl}$* mice were sequenced, and a median of 1615 genes were read out per cell, suggesting the two samples were quite comparable. We performed integration analysis of the control and *Gli1-Cre^{ERT2};Runx2$^{fl/fl}$* sequencing data using Seurat v3. The cells were divided into 19 clusters based on their distinct gene expression profiles (Fig. 3B). Cells color-coded by sample suggested there was not a major shift in the cell distribution between control and *Gli1-Cre^{ERT2};Runx2$^{fl/fl}$* mice (Fig. S5B). Cells in Clusters 0, 1, 3, and 4 were identified as dental papilla cells by marker genes *Slc20a2* and *Msx2* (Fig. 3B),[28,29] while Cluster 15 represented odontoblasts marked by *Dspp* (Fig. S5C). Cluster 2 was identified as dental follicle cells by marker genes *Bmp3* and *Spon1* (Fig. 3B).[30] The other clusters represented dental epithelium (Clusters 9, 11, 12, 13, 14), endothelial cells (Cluster 8), immune cells (Clusters 5, 6, 7, 10, 17), and glia (Clusters 16, 18) (Fig. S5C).

The most enriched genes of each cluster within the dental papilla were used to map the clusters to their anatomic locations. Two marker genes of Cluster 1, *Dio3* and *Itga4*, were found to be expressed in the apical dental mesenchyme (Fig. 3C, D), where root formation initiates, suggesting

cells in Cluster 1 are associated with root formation. We integrated the differentially expressed genes identified in the bulk RNA-seq analysis with their expression profiles revealed by scRNA-seq to verify specific downstream targets of *Runx2*. We identified a number of genes that were enriched in Cluster 1 that had significant differences in signal quantity and intensity, namely *Gli1*, *Pcp4*, *Notum* and *Sfrp2* (Fig. 3E, S6A-D). The differences in the expression levels of these candidate genes were validated by RNAscope *in situ* hybridization (Fig. 4E-T) and qPCR (Fig. S6E-H), and their expression was assessed for overlap with RUNX2 in developing molars (Fig. 4A-D). *Gli1* and *Pcp4* were expressed in the apical region of the dental mesenchyme in control mice, especially close to HERS, while their expression was sharply decreased in *Gli1-Cre^{ERT2};Runx2$^{fl/fl}$* mice (Fig. 4E-L). *Notum* was expressed solely in the progenitors of odontoblast next to HERS in control mice, whereas its expression almost vanished in *Gli1-Cre^{ERT2};Runx2$^{fl/fl}$* mice (Fig. 4M-P). *Sfrp2* expression was found predominantly in the dental follicle in control mice, and its expression was also significantly decreased in *Gli1-Cre^{ERT2};Runx2$^{fl/fl}$* mice (Fig. 4Q-T), therefore most likely to be associated with periodontal tissue development. These findings suggest that integration of data on differentially expressed genes from complementary bulk and single-cell RNA-seq analyses can help to verify downstream targets efficiently. It was interesting to find that *Notum* expression concentrated in the preodontoblast region, which indicates that *Notum* may play an important role in the odontoblastic lineage commitment of the GLI1+ progenitor cells.

Runx2 **determines odontoblastic differentiation of GLI1+ MSCs via inhibition of WNT signaling through a WNT inhibitor, *Notum***

Notum is a recently identified WNT antagonist that acts via inactivation of WNT ligands.[31,32] Since *Notum* expression was almost undetectable in the *Runx2* mutant molars (Fig. 4M-P), we further examined WNT signaling activity using *Axin2* as a readout. We found that *Axin2*

expression was increased in the apical region of the mesenchyme around HERS, especially in the preodontoblast region of *Gli1-Cre^{ERT2};Runx2$^{fl/fl}$* mice, where *Notum* signals vanished (Fig. S7A-D, I), suggesting that loss of *Notum* resulted in upregulation of WNT signaling in the apical dental mesenchyme. We also found that WNT ligands *Wnt3a* and *Wnt4* were expressed in the nearby dental epithelial structure of HERS (Fig. S7E-H). Considering these findings, we hypothesized that NOTUM inactivates WNT ligands WNT3a and WNT4, which are secreted by dental epithelium, thereby mediating the level of WNT activity in the dental mesenchyme that is essential for the odontoblastic lineage commitment of GLI1+ MSCs.

To examine the interaction between *Runx2* and *Notum*, we collected the apical dental mesenchymal tissue from control mandibular first molars at PN7.5 for ATAC-seq. The chromosome view showed there was an open chromatin signal and a MACS2 peak at the promoter region of *Notum* (Fig. 5A) and promoter prediction identified a RUNX2 binding site in the same region, suggesting that *Notum* was actively transcribed and that RUNX2 may regulate its transcription. Chromatin immunoprecipitation (ChIP) analysis revealed that endogenous RUNX2 binds to the genomic loci of *Notum* (Fig. 5B). Our results therefore indicate that RUNX2 directly regulates *Notum* expression to control root development.

Exogenous NOTUM partially rescues the root defects in *Gli1-Cre^{ERT2};Runx2$^{fl/fl}$* mice

Since *Notum* expression is centralized in the preodontoblast region and may guide odontoblastic differentiation, we sought to determine whether *Notum* could rescue the odontoblast differentiation defects we observed in *Gli1-Cre^{ERT2};Runx2$^{fl/fl}$* mice. First we cultured the dental pulp cells from control mouse molars, then added NOTUM protein to the odontoblast differentiation medium. As expected, exogenous NOTUM significantly promoted odontoblast differentiation by activating the odontoblast-specific marker *Dspp* (Fig. 5C-F). Moreover, exogenous NOTUM could rescue the

impaired odontoblast differentiation after *Runx2* siRNA-mediated knockdown *in vitro* (Fig. 5G-J, S8).

We further tested whether ectopic NOTUM protein could rescue the root defects in *Gli1-Cre^{ERT2};Runx2$^{fl/fl}$* mice using kidney capsule transplantation. In control explants, the teeth developed two normal roots. The newly formed root dentin was thick and predentin was detectable, indicating that active dentinogenesis occurred, and the odontoblasts were polarized and columnar (Fig. 6A, D, G). In the *Gli1-Cre^{ERT2};Runx2$^{fl/fl}$* molar explants with BSA beads, the roots were shorter and irregular with thinner dentin, predentin was absent, and odontoblasts were undetectable along with the dentin (Fig. 6B, E, H). In contrast, after treatment with NOTUM beads, the root dentin of *Gli1-Cre^{ERT2};Runx2$^{fl/fl}$* molar explants became more regular, predentin was present, and odontoblast-like cells accumulated at the surface of the dentin, although they were not columnar in shape (Fig. 6C, F, I). Furthermore, there was almost no expression of odontoblast marker *Dspp* in the roots of *Gli1-Cre^{ERT2};Runx2$^{fl/fl}$* molar explants with BSA beads (Fig. 6K, N), compared to the control group (Fig. 6J, M); in contrast, in the *Gli1-Cre^{ERT2};Runx2$^{fl/fl}$* molar explants with NOTUM beads, *Dspp* expression became detectable in the root apical region near the beads, as well as the furcation region (Fig. 6L, O), suggesting that there were some differentiated odontoblasts. However, the root length was not restored after treatment with NOTUM beads (Fig. S9). These results suggest that NOTUM can activate *Dspp* expression *in vitro* and partially rescue the root defects in *Gli1-Cre^{ERT2};Runx2$^{fl/fl}$* mice.

Discussion

During development, progenitor cells play crucial roles in organogenesis. It is therefore important to improve our understanding of the fate control of progenitor cells to advance developmental biology and regenerative medicine. Tooth root development has emerged as an excellent model to study how progenitor cells contribute to organogenesis at late developmental stages. In this study, we discovered that *Runx2*, a transcription factor well known for its role in the fate determination of pluripotent mesenchymal cells committing to the osteoblastic lineage, also defines the stem cell niche and regulates the fate of GLI1+ progenitor cells during tooth root development, partially through activating WNT inhibitor *Notum* expression in the preodontoblast region to trigger the odontoblastic lineage commitment of root progenitor cells. Our results suggest that *Runx2* is important in the cell fate determination of progenitor cells of different origins.

The *Runx2*-mediated regulatory network in controlling tooth development is complex. In early embryonic tooth development, FGF derived from the epithelium induces expression of *Runx2* in the dental mesenchyme, which in turn regulates the expression of mesenchymal *Fgf3* and other downstream targets. These downstream targets then induce *Shh* expression in the epithelial enamel knot to support crown formation.[33] *Runx2*-deficient mice exhibit arrested tooth development at the cap stage.[11] In postnatal stages of crown formation, *Runx2* expression is detectable in ameloblasts during the late secretory and maturation stages, and *Runx2* deficiency in ameloblasts results in enamel hypomineralization, a phenotype seen in CCD patients.[12] *Runx2* expression is not present in HERS (see Fig.1B, F), and loss of epithelial *Runx2* does not affect root elongation and dentin formation,[12] suggesting that epithelial *Runx2* has little impact on the dental mesenchyme. Our study discovered that in tooth root development, *Runx2* expression overlaps with a subpopulation of GLI1+ cells in the dental mesenchyme, but they are not progenitor cells.

Loss of *Runx2* in these GLI1+ cells and their progeny results in severe root developmental defects. We demonstrated that *Runx2* regulates odontoblast differentiation through a key downstream target, *Notum*, in the preodontoblast region of mouse molars, together with other downstream target genes, *Gli1*, *Pcp4*, and *Sfrp2*, to control the fate of root progenitor cells, thus supporting root formation. Our findings expand the understanding of the function of *Runx2* in regulating tooth development and help to elucidate how *Runx2* achieves functional specificity in regulating the development of diverse tissues and organs.

NOTUM deacylates WNTs to suppress signaling activity.[31] As a secreted WNT antagonist, it is crucial in several developmental processes, including vertebrate neural and head induction, bone formation, and tracheal cartilage patterning.[32,34,35] *Notum* null mice develop dentin dysplasia and short tooth roots,[36] indicating that *Notum* functions in tooth root formation. Here, we first illustrated the expression pattern of *Notum* in the preodontoblast region during tooth root development and demonstrated that *Runx2* is an upstream regulator of *Notum*. NOTUM deacylates WNT3a to attenuate WNT/β-catenin signaling, and its expression overlaps with that of *Ainx2* in the developing trachea,[35] which is consistent with our findings that ablation of *Runx2* in developing mouse molars results in diminished *Notum* expression and enhanced WNT/β-catenin signaling, which disturbs the balance between proliferation and differentiation in the apical dental mesenchyme, resulting in root defects. We also propose that Notum influences odontoblast differentiation by inactivating of WNT ligands WNT3a and WNT4, which are secreted by the dental epithelial structure HERS, thus acting as an important mediator in the epithelial-mesenchymal interaction during root development. Moreover, we found that NOTUM could activate expression of the odontoblast marker *Dspp in vitro* and partially rescue the root defects in

Gli1-Cre^{ERT2}*;Runx2*$^{fl/fl}$ mice. These findings suggest that *Notum* is a key regulator of odontoblast differentiation.

The interaction between *Runx2* and WNT signaling pathways has long been studied. *Runx2* regulates osteogenic lineage commitment of suture mesenchymal cells through directly stimulating the expression of WNT signaling genes *Tcf7*, *Wnt10b* and *Wnt1*.[37] Canonical WNT signaling enhances *Runx2* expression to promote osteogenesis through direct binding to the promoter of *Runx2* by TCF-1/Lef1, downstream of β-catenin.[38,39] WNT signaling must be properly regulated during odontogenesis. Inactivating β-catenin in odontoblasts produces molars with a complete absence of roots, due to the disruption of odontoblast differentiation.[40,41] Overexpression of β-catenin in *OC-Cre* mice leads to shortened roots and excessive formation of dentin and cementum.[42,43] However, it has remained unknown how WNT/β-catenin signaling is regulated during odontoblast differentiation. Here for the first time we revealed the important function of the WNT inhibitor NOTUM in this process. We identified that *Runx2* regulates canonical WNT signaling through activating *Notum* in tooth root development, providing insight into the regulatory network that links *Runx2* and the WNT/β-catenin signaling pathway.

Runx2 is also detectable in the periodontal ligament and alveolar bone (see Fig. S2A-C), and we observed severe defects in periodontal tissue in our mutant mice as well, indicating that *Runx2* also regulates other downstream targets to support root development. *Sfrp2* is also a secreted WNT repressor that inhibits canonical WNT signaling by enhancing phosphorylation of β-catenin and downregulating *Axin2*.[44] It also enhances osteogenic differentiation of dental MSCs and helps maintain their survival *in vitro*. Here we found that *Sfrp2* was expressed in the most apical region of the dental papilla and follicle, but not in the preodontoblast region, suggesting that *Sfrp2* may not be a key regulator of odontoblast commitment *in vivo*, but it may still be crucial for the survival

of dental MSCs, as well as for the formation of periodontal tissue. PCP4 is a calmodulin (CaM) regulator protein, and we found that it was expressed in the apical dental mesenchyme, suggesting it may be involved in cell fate determination within this tissue. CaM regulates various cellular functions, including the cell cycle, cell death, ion transport, and neurotransmission.[45] The exact functions of *Sfrp2* and *Pcp4* in regulating tooth root development require further investigation.

GLI1+ cells are a well-established mesenchymal stem cell population in many murine tissues, including bone marrow[46], molar and incisor teeth[8,47], and cranial sutures[48]. Nevertheless, they are heterogeneous. In our scRNA-seq data, we have shown that GLI1+ cells are distributed in different clusters, and we identified that RUNX2+ cells are a subpopulation of GLI1+ cells within the dental mesenchyme. However, these cells do not contribute to root growth. Instead, these RUNX2+ cells appear to play an important role for the differentiation of preodontoblasts during root development. Moreover, loss of *Runx2* in GLI1+ MSCs results in a decrease of GLI1 signaling, suggesting that *Runx2* may be important for maintaining the stem cell niche in developing molars. It will be interesting to learn how these RUNX2+ cells provide feedback to regulate the stem cells. It also remains important for future research to define a more specific *in vivo* marker for mesenchymal stem cells in the developing tooth.

In summary, our study provides *in vivo* evidence of the crucial role of *Runx2* in regulating tooth root formation in a mouse model. This study improves our understanding of how *Runx2* regulates the development of diverse organs in a functionally specific manner. Moreover, we identified several unique downstream targets of *Runx2* in regulating root development, and we highlighted the function of a WNT inhibitor, NOTUM, in odontoblast differentiation. Our discovery yields new insights into the signaling network that regulates tooth root development and may have important implications for approaches to tooth regeneration.

Acknowledgements

We thank Bridget Samuels and Linda Hattemer for critical reading of the manuscript. We acknowledge USC Libraries Bioinformatics Service for assisting with data analysis. The bioinformatics software and computing resources used in the analysis are funded by the USC Office of Research and the USC Libraries. This study was supported by grants from the National Institute of Dental and Craniofacial Research, National Institutes of Health (RO1 DE022503 and RO1 DE025221).

Author contributions

Q.W. and Y.C. designed the study. Q.W. performed most of the experiments, made all figures and analyzed the data. J.J., X.H. and Y.Y. helped to analyze the NGS data. J.F provided critical comments. Y.M and S.C participated in sample collection and mouse surgery. T-V.H. participated in the microCT analysis. Q.W. and Y.C. co-wrote the paper. Y.C. supervised the research.

Competing interests

The authors declare no competing interests.

References

1. Jernvall J, Thesleff I. Reiterative signaling and patterning during mammalian tooth morphogenesis. Mech Develop. 2000/03/15/ 2000;92(1):19-29.
2. Chai Y, Jiang X, Ito Y, Bringas P, Han J, Rowitch DH, et al. Fate of the mammalian cranial neural crest during tooth and mandibular morphogenesis. Development. 2000;127(8):1671.
3. Chai Y, Maxson RE, Jr. Recent advances in craniofacial morphogenesis. Dev Dyn. Sep 2006;235(9):2353-75.
4. Tucker A, Sharpe P. The cutting-edge of mammalian development; how the embryo makes teeth. Nat Rev Genet. Jul 2004;5(7):499-508.
5. Thesleff I. Epithelial-mesenchymal signalling regulating tooth morphogenesis. J Cell Sci. May 1 2003;116(Pt 9):1647-8.
6. Li J, Parada C, Chai Y. Cellular and molecular mechanisms of tooth root development. Development. Feb 1 2017;144(3):374-84.
7. Ono W, Sakagami N, Nishimori S, Ono N, Kronenberg HM. Parathyroid hormone receptor signalling in osterix-expressing mesenchymal progenitors is essential for tooth root formation. Nat Commun. Apr 12 2016;7:11277.
8. Feng J, Jing J, Li J, Zhao H, Punj V, Zhang T, et al. BMP signaling orchestrates a transcriptional network to control the fate of mesenchymal stem cells in mice. Development. Jul 15 2017;144(14):2560-9.
9. Komori T. Regulation of bone development and extracellular matrix protein genes by RUNX2. Cell Tissue Res. Jan 2010;339(1):189-95.
10. Mundlos S, Otto F, Mundlos C, Mulliken JB, Aylsworth AS, Albright S, et al. Mutations involving the transcription factor CBFA1 cause cleidocranial dysplasia. Cell. May 30 1997;89(5):773-9.
11. D'Souza RN, Aberg T, Gaikwad J, Cavender A, Owen M, Karsenty G, et al. Cbfa1 is required for epithelial-mesenchymal interactions regulating tooth development in mice. Development. Jul 1999;126(13):2911-20.
12. Chu Q, Gao Y, Gao X, Dong Z, Song W, Xu Z, et al. Ablation of Runx2 in Ameloblasts Suppresses Enamel Maturation in Tooth Development. Sci Rep. Jun 25 2018;8(1):9594.
13. Ahn S, Joyner AL. Dynamic changes in the response of cells to positive hedgehog signaling during mouse limb patterning. Cell. Aug 20 2004;118(4):505-16. Epub 2004/08/19.
14. Madisen L, Zwingman TA, Sunkin SM, Oh SW, Zariwala HA, Gu H, et al. A robust and high-throughput Cre reporting and characterization system for the whole mouse brain. Nature neuroscience. Jan 2010;13(1):133-40. Epub 2009/12/22.
15. Takarada T, Hinoi E, Nakazato R, Ochi H, Xu C, Tsuchikane A, et al. An analysis of skeletal development in osteoblast-specific and chondrocyte-specific runt-related transcription factor-2 (Runx2) knockout mice. J Bone Miner Res. Oct 2013;28(10):2064-9.
16. Bai CB, Auerbach W, Lee JS, Stephen D, Joyner AL. Gli2, but not Gli1, is required for initial Shh signaling and ectopic activation of the Shh pathway. Development. Oct 2002;129(20):4753-61. Epub 2002/10/04.
17. Chen JQ, Tu XL, Esen E, Joeng KS, Lin CX, Arbeit JM, et al. WNT7B Promotes Bone Formation in part through mTORC1. Plos Genet. Jan 2014;10(1).
18. Perl AK, Wert SE, Nagy A, Lobe CG, Whitsett JA. Early restriction of peripheral and proximal cell lineages during formation of the lung. Proc Natl Acad Sci U S A. Aug 6 2002;99(16):10482-7. Epub 2002/07/30.
19. Lu Y, Xie Y, Zhang S, Dusevich V, Bonewald LF, Feng JQ. DMP1-targeted Cre expression in odontoblasts and osteocytes. J Dent Res. Apr 2007;86(4):320-5. Epub 2007/03/27.

20. Spandidos A, Wang X, Wang H, Seed B. PrimerBank: a resource of human and mouse PCR primer pairs for gene expression detection and quantification. Nucleic Acids Research. 2009;38(suppl_1):D792-D9.
21. Butler A, Hoffman P, Smibert P, Papalexi E, Satija R. Integrating single-cell transcriptomic data across different conditions, technologies, and species. Nature Biotechnology. 2018/05/01 2018;36(5):411-20.
22. Stuart T, Butler A, Hoffman P, Hafemeister C, Papalexi E, Mauck WM, 3rd, et al. Comprehensive Integration of Single-Cell Data. Cell. Jun 13 2019;177(7):1888-902 e21.
23. Buenrostro JD, Wu B, Chang HY, Greenleaf WJ. ATAC-seq: A Method for Assaying Chromatin Accessibility Genome-Wide. Curr Protoc Mol Biol. Jan 5 2015;109:21 9 1- 9 9.
24. Heinz S, Benner C, Spann N, Bertolino E, Lin YC, Laslo P, et al. Simple combinations of lineage-determining transcription factors prime cis-regulatory elements required for macrophage and B cell identities. Molecular cell. May 28 2010;38(4):576-89. Epub 2010/06/02.
25. Lacerda-Pinheiro S, Dimitrova-Nakov S, Harichane Y, Souyri M, Petit-Cocault L, Legres L, et al. Concomitant multipotent and unipotent dental pulp progenitors and their respective contribution to mineralised tissue formation. Eur Cell Mater. May 24 2012;23:371-86.
26. Camilleri S, McDonald F. Runx2 and dental development. Eur J Oral Sci. Oct 2006;114(5):361-73.
27. Komori T, Yagi H, Nomura S, Yamaguchi A, Sasaki K, Deguchi K, et al. Targeted disruption of Cbfa1 results in a complete lack of bone formation owing to maturational arrest of osteoblasts. Cell. May 30 1997;89(5):755-64.
28. Yamashiro T, Tummers M, Thesleff I. Expression of Bone Morphogenetic Proteins and Msx Genes during Root Formation. J Dent Res. 2003/03/01 2003;82(3):172-6.
29. Zhao D, Vaziri Sani F, Nilsson J, Rodenburg M, Stocking C, Linde A, et al. Expression of Pit2 sodium-phosphate cotransporter during murine odontogenesis is developmentally regulated. European Journal of Oral Sciences. 2006/12/01 2006;114(6):517-23.
30. Takahashi A, Nagata M, Gupta A, Matsushita Y, Yamaguchi T, Mizuhashi K, et al. Autocrine regulation of mesenchymal progenitor cell fates orchestrates tooth eruption. Proc Natl Acad Sci U S A. Jan 8 2019;116(2):575-80.
31. Kakugawa S, Langton PF, Zebisch M, Howell S, Chang TH, Liu Y, et al. Notum deacylates Wnt proteins to suppress signalling activity. Nature. Mar 12 2015;519(7542):187-92.
32. Zhang X, Cheong SM, Amado NG, Reis AH, MacDonald BT, Zebisch M, et al. Notum is required for neural and head induction via Wnt deacylation, oxidation, and inactivation. Dev Cell. Mar 23 2015;32(6):719-30.
33. Aberg T, Wang XP, Kim JH, Yamashiro T, Bei M, Rice R, et al. Runx2 mediates FGF signaling from epithelium to mesenchyme during tooth morphogenesis. Dev Biol. Jun 1 2004;270(1):76-93.
34. Brommage R, Liu J, Vogel P, Mseeh F, Thompson AY, Potter DG, et al. NOTUM inhibition increases endocortical bone formation and bone strength. Bone Res. 2019;7:2.
35. Gerhardt B, Leesman L, Burra K, Snowball J, Rosenzweig R, Guzman N, et al. Notum attenuates Wnt/beta-catenin signaling to promote tracheal cartilage patterning. Dev Biol. Apr 1 2018;436(1):14-27.
36. Vogel P, Read RW, Hansen GM, Powell DR, Kantaputra PN, Zambrowicz B, et al. Dentin Dysplasia in Notum Knockout Mice. Vet Pathol. Jul 2016;53(4):853-62.
37. Qin X, Jiang Q, Miyazaki T, Komori T. Runx2 regulates cranial suture closure by inducing hedgehog, Fgf, Wnt, and Pthlh signaling pathway gene expression in suture mesenchymal cells. Hum Mol Genet. Nov 16 2018.
38. Gaur T, Lengner CJ, Hovhannisyan H, Bhat RA, Bodine PV, Komm BS, et al. Canonical WNT signaling promotes osteogenesis by directly stimulating Runx2 gene expression. J Biol Chem. Sep 30 2005;280(39):33132-40. Epub 2005/07/27.

39. Dong YF, Soung do Y, Schwarz EM, O'Keefe RJ, Drissi H. Wnt induction of chondrocyte hypertrophy through the Runx2 transcription factor. Journal of cellular physiology. Jul 2006;208(1):77-86. Epub 2006/04/01.
40. Kim TH, Bae CH, Lee JC, Ko SO, Yang X, Jiang R, et al. beta-catenin is required in odontoblasts for tooth root formation. J Dent Res. Mar 2013;92(3):215-21.
41. Zhang R, Yang G, Wu X, Xie J, Yang X, Li T. Disruption of Wnt/beta-catenin signaling in odontoblasts and cementoblasts arrests tooth root development in postnatal mouse teeth. Int J Biol Sci. 2013;9(3):228-36.
42. Bae CH, Lee JY, Kim TH, Baek JA, Lee JC, Yang X, et al. Excessive Wnt/beta-catenin signaling disturbs tooth-root formation. J Periodontal Res. Aug 2013;48(4):405-10.
43. Kim TH, Lee JY, Baek JA, Lee JC, Yang X, Taketo MM, et al. Constitutive stabilization of ss-catenin in the dental mesenchyme leads to excessive dentin and cementum formation. Biochem Biophys Res Commun. Sep 9 2011;412(4):549-55.
44. Jin L, Cao Y, Yu G, Wang J, Lin X, Ge L, et al. SFRP2 enhances the osteogenic differentiation of apical papilla stem cells by antagonizing the canonical WNT pathway. Cell Mol Biol Lett. 2017;22:14.
45. Berchtold MW, Villalobo A. The many faces of calmodulin in cell proliferation, programmed cell death, autophagy, and cancer. Biochimica et Biophysica Acta (BBA) - Molecular Cell Research. 2014/02/01/ 2014;1843(2):398-435.
46. Schneider RK, Mullally A, Dugourd A, Peisker F, Hoogenboezem R, Van Strien PMH, et al. Gli1+ Mesenchymal Stromal Cells Are a Key Driver of Bone Marrow Fibrosis and an Important Cellular Therapeutic Target. Cell Stem Cell. 2017/06/01/ 2017;20(6):785-800.e8.
47. Zhao H, Feng J, Seidel K, Shi S, Klein O, Sharpe P, et al. Secretion of shh by a neurovascular bundle niche supports mesenchymal stem cell homeostasis in the adult mouse incisor. Cell Stem Cell. Feb 6 2014;14(2):160-73.
48. Zhao H, Feng J, Ho TV, Grimes W, Urata M, Chai Y. The suture provides a niche for mesenchymal stem cells of craniofacial bones. Nat Cell Biol. Apr 2015;17(4):386-96.

Figure Legends

Figure 1. Colocalization of RUNX2 and GLI1+ MSCs and their progeny in developing roots.

(A-D) RUNX2 (green) and GLI1 (stained by β-gal in red) co-immunofluorescence of sagittal sections of mandibular molars from PN3.5 heterozygous *Gli1-LacZ* mice. (E-L) RUNX2 immunofluorescence (green) and visualization of tdTomato (red) of sagittal sections of mandibular molars from *Gli1-Cre^{ERT2};tdTomato$^{fl/+}$* mice at PN7.5 (E-H) and PN21.5 (I-L) after induction at PN3.5. The progeny of the GLI1+ lineage present red. Boxes in A, E and I are enlarged in B-D, F-H and J-L, respectively. White dashed lines outline HERS; arrows indicate co-localization. Scale bars: 100 μm.

Figure 2. Loss of *Runx2* in GLI1+ MSCs results in root development defects.

(A-D) MicroCT images of *Runx2$^{fl/fl}$* control (A, B) and *Gli1-Cre^{ERT2};Runx2$^{fl/fl}$* (C, D) mandibular molars at PN21.5. (E-J) H&E staining of *Runx2$^{fl/fl}$* control (E-G) and *Gli1-Cre^{ERT2};Runx2$^{fl/fl}$* (H-J) mandibular molars at PN21.5. Boxed areas in E and H are shown magnified in F-G and I-J, respectively. D = dentin; DP = dental pulp; OD = odontoblast; C = cementoblast; PDL = periodontal ligament; AB = alveolar bone. Yellow arrowheads indicate the absence of cementoblasts and periodontal ligament. (K-P) *Dspp in situ* hybridization (red) at PN21.5 (K, N), and Ki67 immunofluorescence (red) indicating proliferating cells at PN7.5 (L, M, O and P) in sagittal sections of mandibular molars in *Runx2$^{fl/fl}$* control and *Gli1-Cre^{ERT2};Runx2$^{fl/fl}$* mice. Arrows in K, M and P indicate positive signals; arrowheads in N indicate absence of signal. Boxes in L and O are enlarged in M and P, respectively. Dashed white lines outline HERS. Scale bars: A-D, 400 μm; all others, 100 μm.

Figure 3. Integrated analysis of bulk RNA-seq and scRNA-seq reveals specific downstream targets of *Runx2*.

(A) Bulk RNA-seq revealed that 219 genes were upregulated and 208 genes were downregulated with > 1.8-fold change ($p < 0.05$) upon *Runx2* deletion, represented here by volcano plot and heatmap. (B) UMAP plots showed 19 clusters within PN7.5 molars after integration of the *Runx2*$^{fl/fl}$ control and *Gli1-Cre*^{ERT2}*;Runx2*$^{fl/fl}$ scRNA sequencing data with Seurat v3. Different clusters represent different cell types in the mouse molar, defined by expression of known marker genes. Dashed lines outline clusters representing the same cell type. Clusters 0,1,3,4,15: dental papilla cells and odontoblasts. Cluster 2: dental follicle cells. The feature plot of the first gene in the list is shown. (C, D) Cluster 1 maps to the apical region of dental mesenchyme by 2 marker genes, *Dio3* (C), and *Itga4* (D). Dashed white lines outline tooth, arrows indicate positive signals. Scale bars: 100 μm. (E) Feature plots and box plots of four differentially expressed genes mapping to cluster 1. They were identified as potential downstream targets of *Runx2*. The differences in expression levels were consistent between feature plots of scRNA-seq and box plots of bulk RNA-seq.

Figure 4. *In vivo* validation of putative downstream targets upon deletion of *Runx2* in the dental mesenchyme.

RUNX2 immunofluorescence (A-D) and RNAscope *in situ* hybridization (red) of *Gli1* (E-H), *Pcp4* (I-L), *Notum* (M-P), and *Sfrp2* (Q-T) of sagittal sections of mandibular molars from PN7.5 *Runx2*$^{fl/fl}$ control and *Gli1-Cre*^{ERT2}*;Runx2*$^{fl/fl}$ mice. The boxed area is enlarged on the right. Dashed lines outline HERS. Arrowhead indicates positive signals; asterisks indicate altered staining in targeted region of mutant samples. N=3 sections were examined from multiple littermate mice per group. Scale bars: 100 μm.

Figure 5. *Notum* is a direct target of RUNX2 and activates the expression of odontoblast marker *Dspp in vitro*.

(A) Genome browser snapshots representing the peak of ATAC-seq from PN7.5 control mouse molars co-localized with the RUNX2 binding site at the promoter region of *Notum*. (B) ChIP analysis revealed the binding of endogenous RUNX2 to the genomic loci of *Notum*. DNA before immunoprecipitation (input) and after immunoprecipitation with an anti-RUNX2 or rabbit IgG was amplified by qPCR using primers that amplify the regions containing RUNX2-binding motifs in the *Notum* promoter. The value of input was defined as 1, and relative levels are shown. (C-J) RNAscope *in situ* hybridization (red) and qPCR of *Dspp* in cultured dental pulp cells treated with control growth media (CM), odontoblastic media (OM), and OM + NOTUM protein (C-F), as well as OM + control siRNA, OM + *Runx2* siRNA, and OM + *Runx2* siRNA + NOTUM protein (G-J), insets in figures C-E and G-I were enlarged images of the cells pointed by arrows in the same image. **$p < 0.01$. Scale bars: 25 μm.

Figure 6. Ectopic NOTUM partially rescues the root defect in *Gli1-Cre^{ERT2};Runx2$^{fl/fl}$* mice.

H&E staining (A-I) and RNAscope *in situ* hybridization of *Dspp* (J-O) of sagittal sections of tooth germs from *Runx2$^{fl/fl}$* control and *Gli1-Cre^{ERT2};Runx2$^{fl/fl}$* mice cultured for 3 weeks under kidney capsules with BSA or NOTUM beads. The control explants developed well; two roots with columnar odontoblasts, thick dentin, and predentin are identifiable (A, D, G). In *Gli1-Cre^{ERT2};Runx2$^{fl/fl}$* molars treated with BSA beads (B, E, H), the root dentin is irregular, and predentin is unseen, arrowheads indicate there are few odontoblast-like cells along with the dentin, some cells are embedded into the dentin. After treatment with NOTUM beads (C, F, I), the root dentin became more regular with detectable predentin, and many odontoblast-like cells accumulated at the surface of the dentin (indicated by black arrows). *Dspp* expression is strong in

control samples (J, M), while in *Gli1-Cre^{ERT2};Runx2$^{fl/fl}$* molars treated with BSA beads (K, N), there are only a few positive signals. Following treatment with NOTUM beads, *Dspp* is detectable in the apical region (L) and furcation region (O). Insets in J, K and L are lower magnification images of the same sample. White arrows indicate positive signal; asterisks indicate absence of signal. D = dentin; PD = predentin; DP = dental pulp; OD = odontoblast; B=bead. N=5 samples were collected and analyzed for each group. Scale bars: 100 μm.

Supplemental Figure 1. RUNX2+ cells are not root progenitor cells in the dental mesenchyme.

Lineage tracing of PN3.5 to PN7.5 RUNX2+ cells using *Runx2-rtTA;Teto-Cre;Tdt*$^{fl/+}$ mice. (A, B) Immediately after labeling at PN7.5, RUNX2+ cells are located in the apical region of dental papilla, dental follicle, and some odontoblasts. (C, D) At PN21.5, the progeny of the RUNX2+ lineage remain red, and are only apparent in a few odontoblasts and pulp cells. Boxes in A and C were enlarged in B and D, respectively. Scale bars: 200 μm.

Supplemental Figure 2. Efficient ablation of *Runx2* results in a differentiation defect in the GLI1+ cell lineage.

(A-F) RUNX2 immunofluorescence (green) and visualization of tdTomato (red) of sagittal sections of mandibular molars from PN21.5 control (A-C) and *Gli1-Cre*^{ERT2}*;Runx2*$^{fl/fl}$*;tdTomato* $^{fl/+}$ mice (D-F) induced at PN3.5. The progeny of the Gli1 lineage appear red. Boxes in A and D are shown magnified in B-C and E-F, respectively. Arrows indicate positive RUNX2 signals and arrowheads indicate absence of signal; asterisk indicates GLI1 derivatives in the periapical region. Scale bars: 100 μm. (G) Quantitation analysis of root length (cementoenamel junction to root apex) of mandibular first molars at PN21.5. (H) qPCR of *Dspp* from root pulp tissue of mandibular first molars from PN21.5 *Runx2*$^{fl/fl}$ control and *Gli1-Cre*^{ERT2}*;Runx2*$^{fl/fl}$ mice. (I) Quantitation of Ki67+ cells in dental papilla (percentage of Ki67+ cells out of total cells in dental papilla).

Supplemental Figure 3. *Gli1-Cre*^{ERT2}*;Runx2*$^{fl/fl}$ mice develop a CCD-like phenotype.

(A-I) MicroCT images of the skull (A, B, E, F), clavicle (C, G) and mandible (D, H), and quantitative analysis (I) of 6-week-old *Runx2*$^{fl/fl}$ control and *Gli1-Cre*^{ERT2}*;Runx2*$^{fl/fl}$ mice induced at PN3.5. Arrow indicates delayed closure of sutures; asterisk indicates normal sutures; red points in B, D, F and H are the landmarks used to measure the skull length and mandible length in I.

Supplemental Figure 4. Root development is unaffected in heterozygous mutant mice or upon deletion of *Runx2* in odontoblasts.

MicroCT images (A, B, D, E, G and H) and H&E staining (C, F and I) of mandibular molars from PN21.5 *Runx2*$^{fl/fl}$ control (A-C), *Gli1-Cre*^{ERT2}*;Runx2*$^{fl/+}$ (D-F), and *Dmp1-Cre;Runx2*$^{fl/fl}$ (G-I) mice. Tamoxifen was administrated to *Gli1-Cre*^{ERT2}*;Runx2*$^{fl/+}$ mice at PN3.5. N=3 samples were examined for each group. Scale bars: 200 μm.

Supplemental Figure 5. Integrated analysis of scRNA-seq reveals different cell types in PN7.5 mouse molar.

(A, B) UMAP plots of mandibular first molar cells from PN7.5 *Runx2*$^{fl/fl}$ control and *Gli1-Cre*^{ERT2}*;Runx2*$^{fl/fl}$ mice colored by cell type (A) and dataset (B) after integration with Seurat v3. (C) Different clusters represent different cell types in PN7.5 mouse molar, defined by expression of known marker genes (the feature plot of the first gene in the list is shown). Dots: individual cells. Dashed lines outline clusters representing the same cell type. Blue: high expression; grey: no expression.

Supplemental Figure 6. Validation of *Runx2* target genes by violin plot and qPCR.

(A-D) Violin plots from scRNA-seq revealed the different expression levels of *Runx2* target genes in dental mesenchyme (clusters 0-4) and odontoblasts (cluster 15). (E-H) qPCR of *Runx2* target genes from apical tissue of mandibular first molars from PN7.5 *Runx2*$^{fl/fl}$ control and *Gli1-Cre*^{ERT2}*;Runx2*$^{fl/fl}$ mice..

Supplemental Figure 7. WNT signaling activity in the apical dental mesenchyme

(A-D) RNAscope *in situ* hybridization of *Axin2* (red) on sagittal sections of mandibular molars from PN7.5 *Runx2*$^{fl/fl}$ control (A, B) and *Gli1-Cre*^{ERT2}*;Runx2*$^{fl/fl}$ (C, D) mice. (E-H) RNAscope *in situ* hybridization (red) of *Wnt3a* (E, F) and *Wnt4* (G, H) of sagittal sections of PN7.5 control mandibular molars. The boxed areas in A, C, E and G are enlarged in B, D, F and H, respectively. Dashed lines outline HERS; arrowheads indicate positive signals. Scale bars: 100 μm. (I) qPCR of *Ainx2* from apical tissue of mandibular first molars from PN7.5 *Runx2*$^{fl/fl}$ control and *Gli1-Cre*^{ERT2}*;Runx2*$^{fl/fl}$ mice.

Supplemental Figure 8. Knockdown efficiency by *Runx2* siRNA on mouse dental pulp cells.

Mouse dental pulp cells were transfected with three *Runx2* siRNAs. qPCR confirmed that *Runx2* siRNA10 exhibited the highest knockdown efficiency and was therefore used in the following experiment. Two-tailed Student's t tests were used to compare the treatment group to the negative siRNA group; P values are shown on the top of each group.

Supplemental Figure 9. Root length is not restored after treatment with NOTUM beads in transplanted *Gli1-Cre*^{ERT2}*;Runx2*$^{fl/fl}$ molars.

Quantification of tooth root length from tooth germs of *Runx2*$^{fl/fl}$ control and *Gli1-Cre*^{ERT2}*;Runx2*$^{fl/fl}$ mice cultured for 3 weeks under kidney capsules with BSA or NOTUM beads.

Figure 1

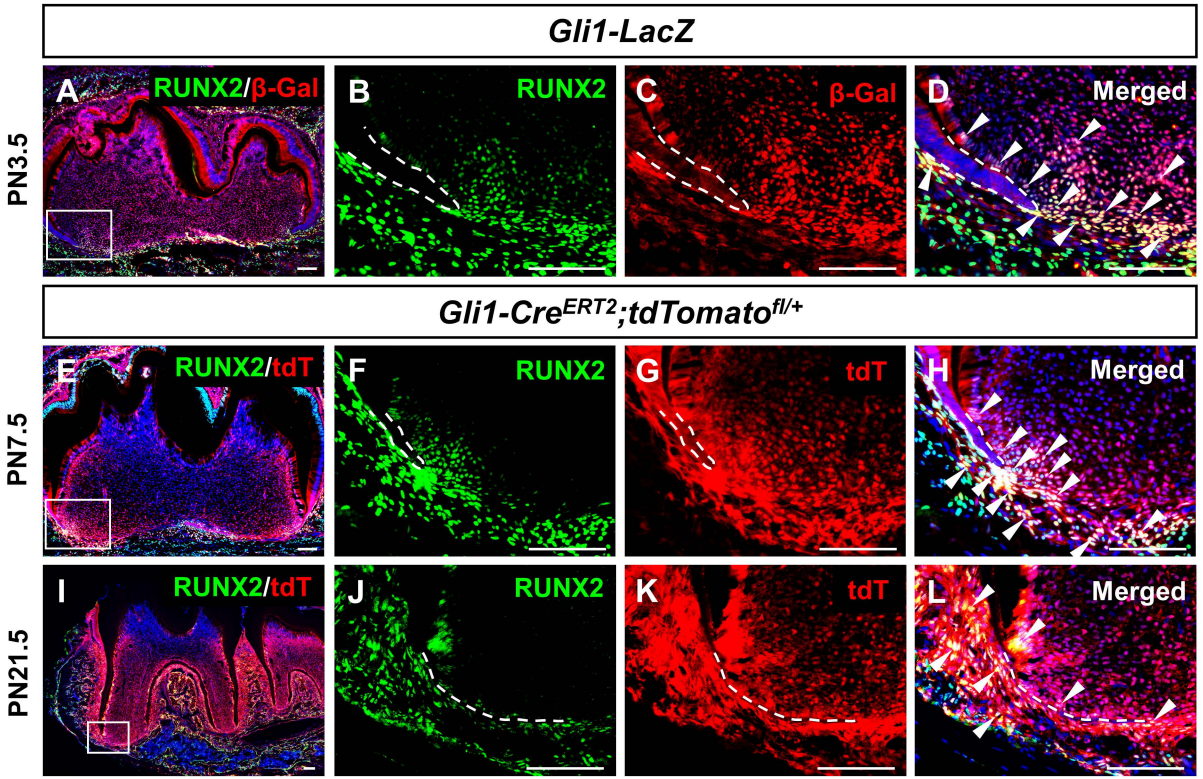
Gli1-LacZ
PN3.5
A
RUNX2/β-Gal
B
RUNX2
C
β-Gal
D
Merged
Gli1-Cre^ERT2;tdTomato^fl/+
PN7.5
E
RUNX2/tdT
F
RUNX2
G
tdT
H
Merged
PN21.5
I
RUNX2/tdT
J
RUNX2
K
tdT
L
Merged

Figure 2

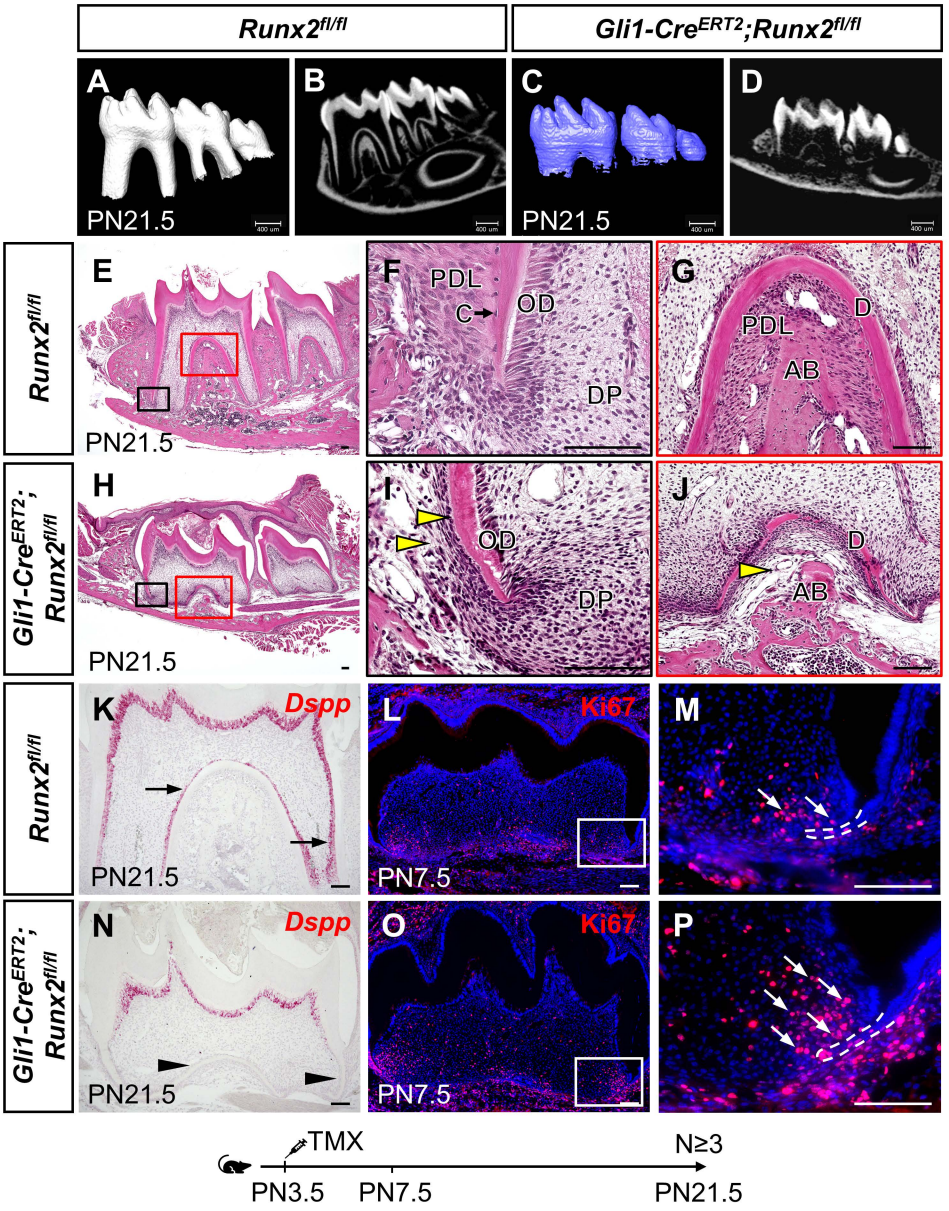
Runx2fl/fl
Gli1-CreERT2;Runx2fl/fl
A
B
C
D
PN21.5
PN21.5
Runx2fl/fl
E
F
G
PN21.5
PDL
C
OD
DP
PDL
D
AB
Gli1-CreERT2; Runx2fl/fl
H
I
J
PN21.5
OD
DP
D
AB
Runx2fl/fl
K
L
M
Dspp
Ki67
PN21.5
PN7.5
Gli1-CreERT2; Runx2fl/fl
N
O
P
Dspp
Ki67
PN21.5
PN7.5
TMX
N≥3
PN3.5
PN7.5
PN21.5

Figure 3

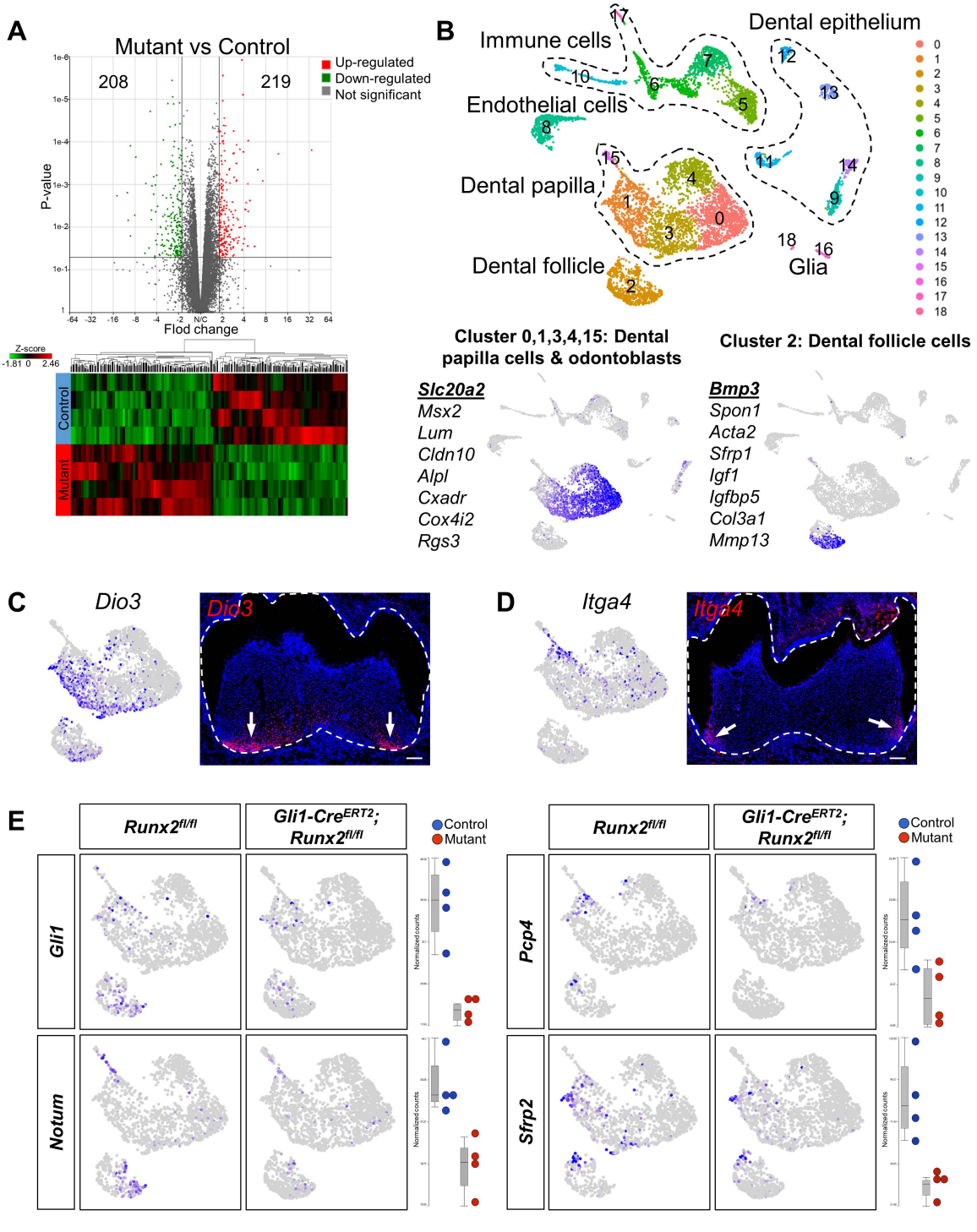
A
Mutant vs Control
208
219
Up-regulated
Down-regulated
Not significant
P-value
Flod change
Z-score
Control
Mutant
B
Immune cells
Dental epithelium
Endothelial cells
Dental papilla
Dental follicle
Glia
Cluster 0,1,3,4,15: Dental papilla cells & odontoblasts
Cluster 2: Dental follicle cells
Slc20a2
Msx2
Lum
Cldn10
Alpl
Cxadr
Cox4i2
Rgs3
Bmp3
Spon1
Acta2
Sfrp1
Igf1
Igfbp5
Col3a1
Mmp13
C
Dio3
D
Itga4
E
Runx2fl/fl
Gli1-CreERT2; Runx2fl/fl
Control
Mutant
Gli1
Notum
Pcp4
Sfrp2
Normalized counts

Figure 4

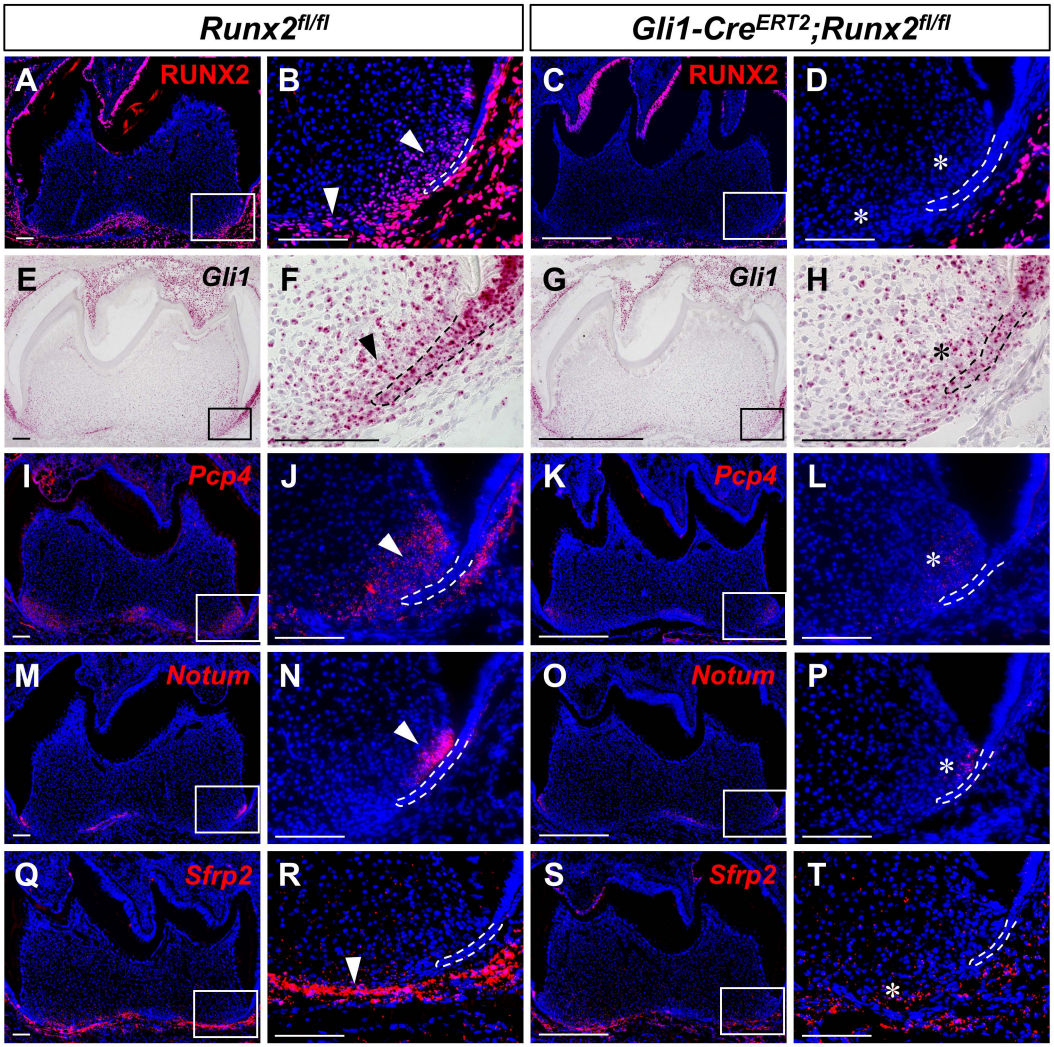
Runx2fl/fl
Gli1-CreERT2;Runx2fl/fl
A
RUNX2
B
C
RUNX2
D
E
Gli1
F
G
Gli1
H
I
Pcp4
J
K
Pcp4
L
M
Notum
N
O
Notum
P
Q
Sfrp2
R
S
Sfrp2
T

Figure 5

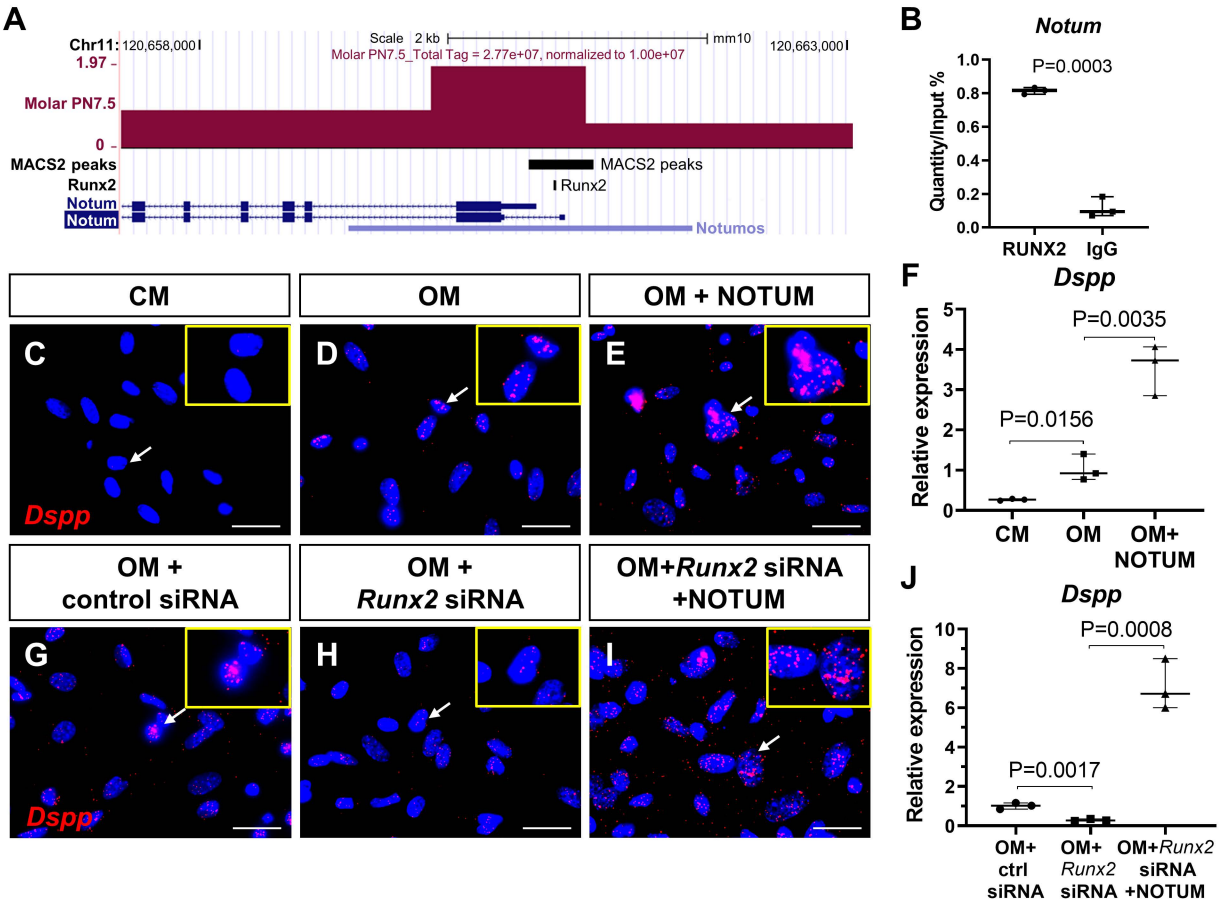
A
Chr11: 120,658,000
1.97
Molar PN7.5
0
MACS2 peaks
Runx2
Notum
Notum
Scale 2 kb
mm10
Molar PN7.5_Total Tag = 2.77e+07, normalized to 1.00e+07
120,663,000
MACS2 peaks
Runx2
Notumos
B
Notum
P=0.0003
Quantity/Input %
RUNX2
IgG
CM
OM
OM + NOTUM
C
D
E
Dspp
F
Dspp
P=0.0035
P=0.0156
Relative expression
CM
OM
OM+ NOTUM
OM + control siRNA
OM + Runx2 siRNA
OM+Runx2 siRNA +NOTUM
G
H
I
Dspp
J
Dspp
P=0.0008
P=0.0017
Relative expression
OM+ ctrl siRNA
OM+ Runx2 siRNA
OM+Runx2 siRNA +NOTUM

Figure 6

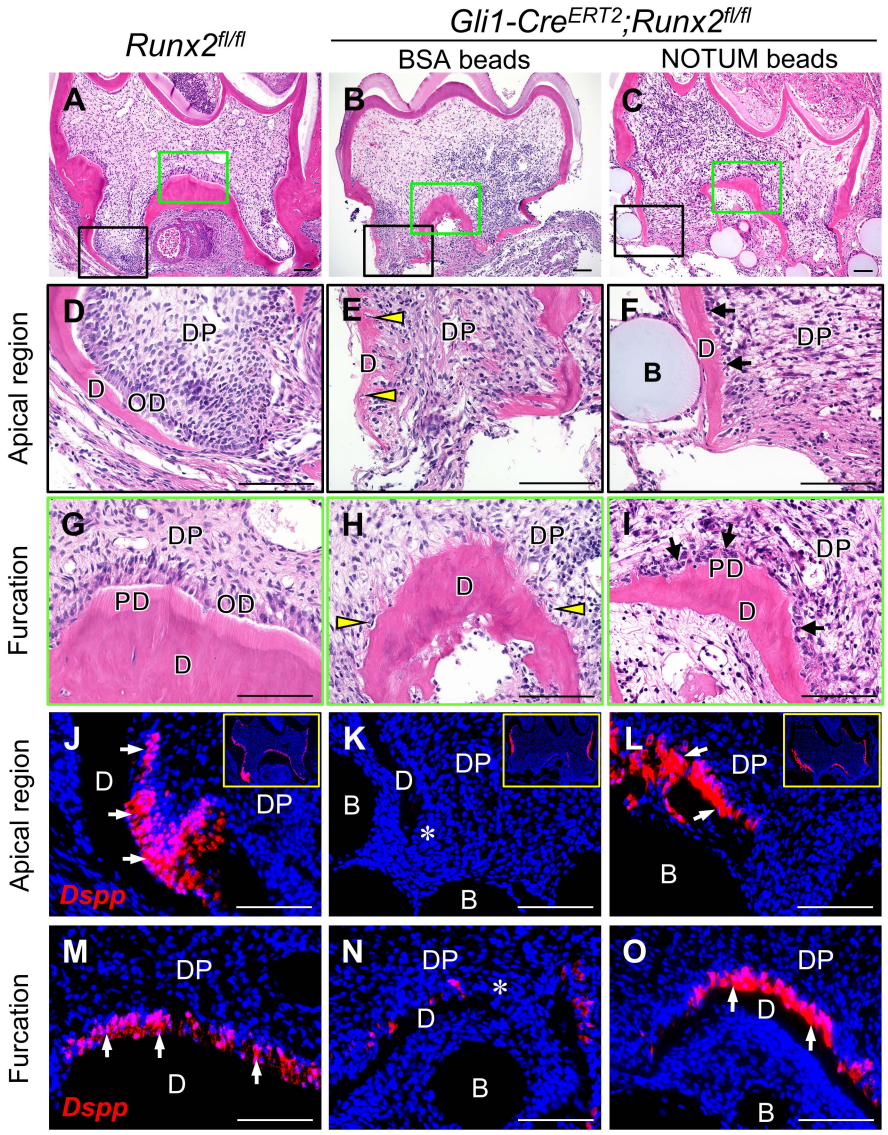
Runx2fl/fl
Gli1-CreERT2;Runx2fl/fl
BSA beads
NOTUM beads
A
B
C
Apical region
D
DP
D
OD
E
DP
D
F
B
D
DP
Furcation
G
DP
PD
OD
D
H
DP
D
I
PD
DP
D
Apical region
J
D
DP
Dspp
K
DP
D
B
*
B
L
DP
B
Furcation
M
DP
D
Dspp
N
DP
*
D
B
O
DP
D
B

S-Figure 1

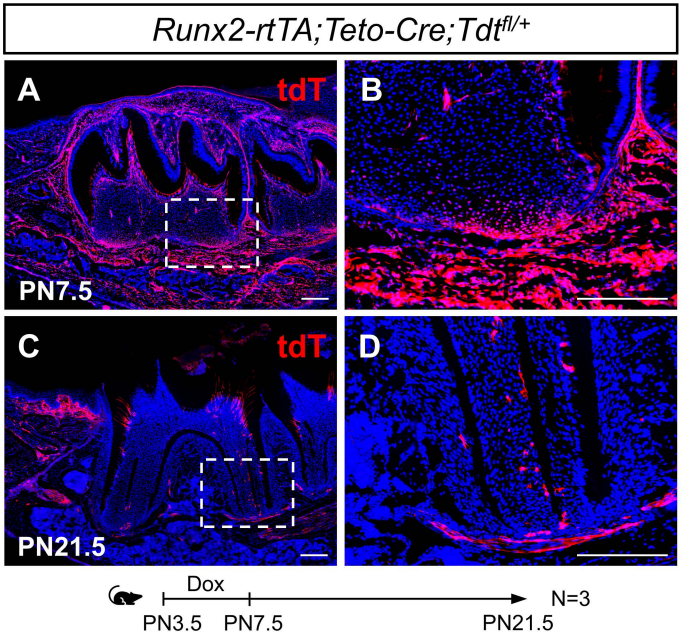
Runx2-rtTA;Teto-Cre;Tdt^fl/+
A
tdT
PN7.5
B
C
tdT
PN21.5
D
Dox
PN3.5
PN7.5
PN21.5
N=3

S-Figure 2

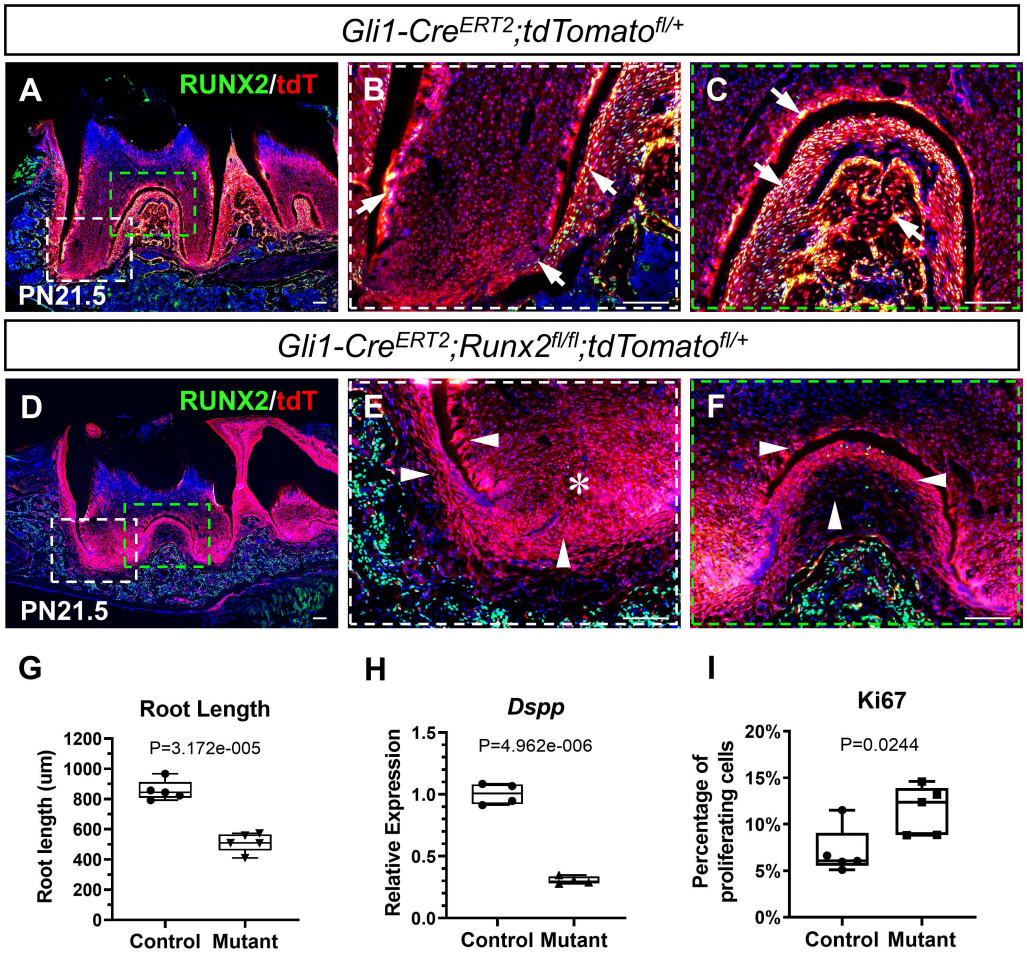
Gli1-CreERT2;tdTomatofl/+
A
RUNX2/tdT
PN21.5
B
C
Gli1-CreERT2;Runx2fl/fl;tdTomatofl/+
D
RUNX2/tdT
PN21.5
E
F
G
Root Length
P=3.172e-005
Root length (um)
1200
1000
800
600
400
200
0
Control
Mutant
H
Dspp
P=4.962e-006
Relative Expression
1.5
1.0
0.5
0.0
Control
Mutant
I
Ki67
P=0.0244
Percentage of proliferating cells
20%
15%
10%
5%
0%
Control
Mutant

S-Figure 3

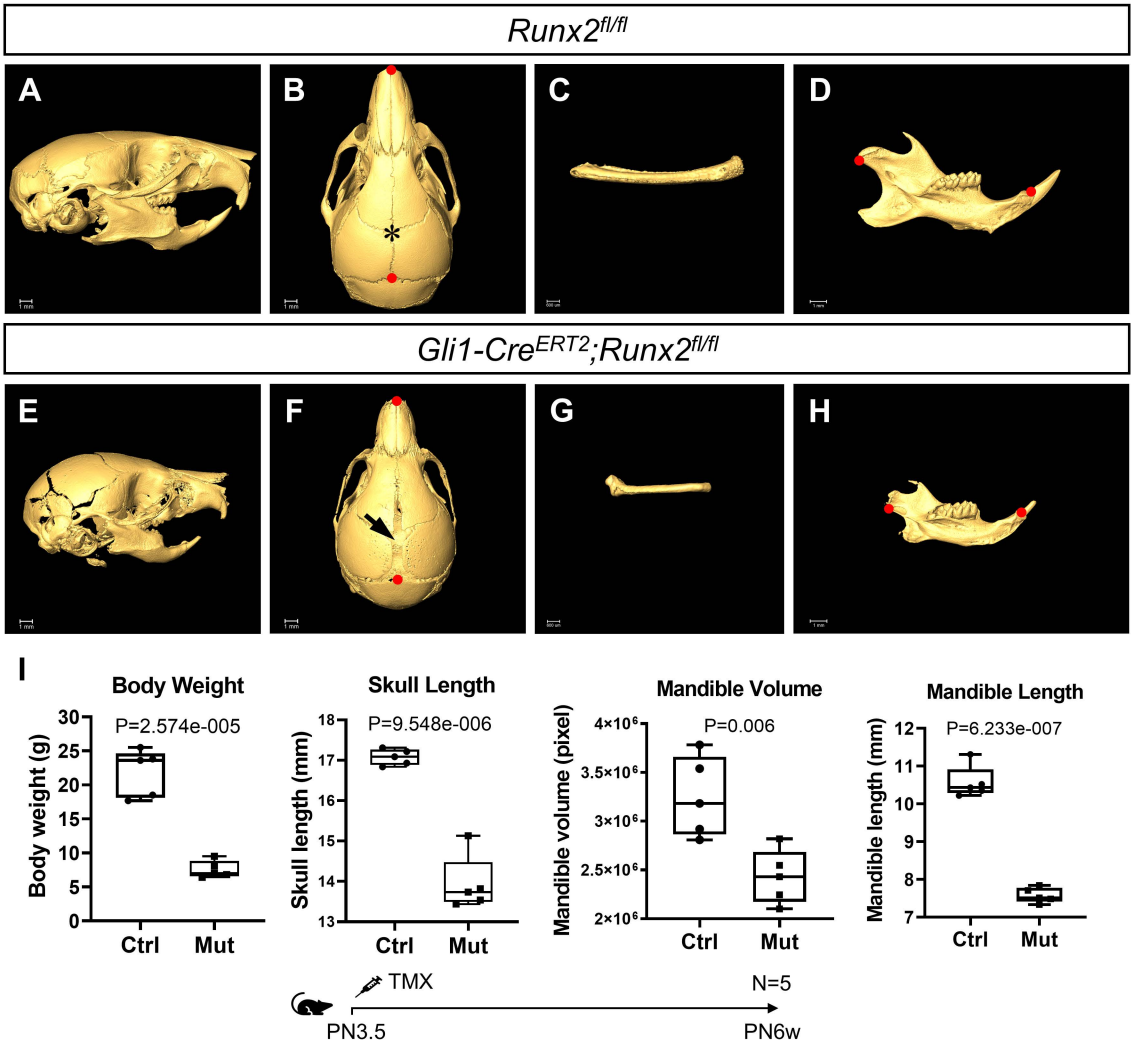
Runx2fl/fl
A
B
C
D
Gli1-CreERT2;Runx2fl/fl
E
F
G
H
I
Body Weight
P=2.574e-005
Body weight (g)
Ctrl
Mut
Skull Length
P=9.548e-006
Skull length (mm)
Mandible Volume
P=0.006
Mandible volume (pixel)
Mandible Length
P=6.233e-007
Mandible length (mm)
TMX
N=5
PN3.5
PN6w

S-Figure 4

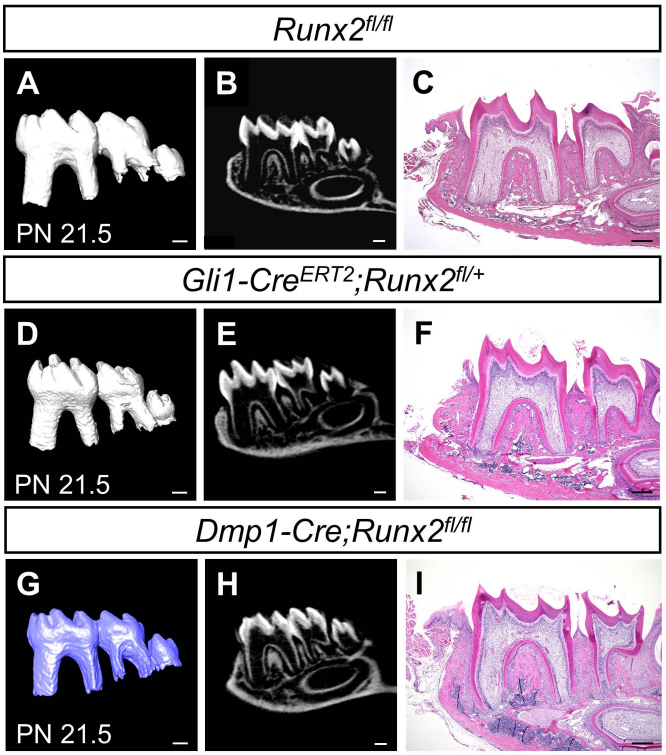
Runx2fl/fl
A
B
C
PN 21.5
Gli1-CreERT2;Runx2fl/+
D
E
F
PN 21.5
Dmp1-Cre;Runx2fl/fl
G
H
I
PN 21.5

S-Figure 5

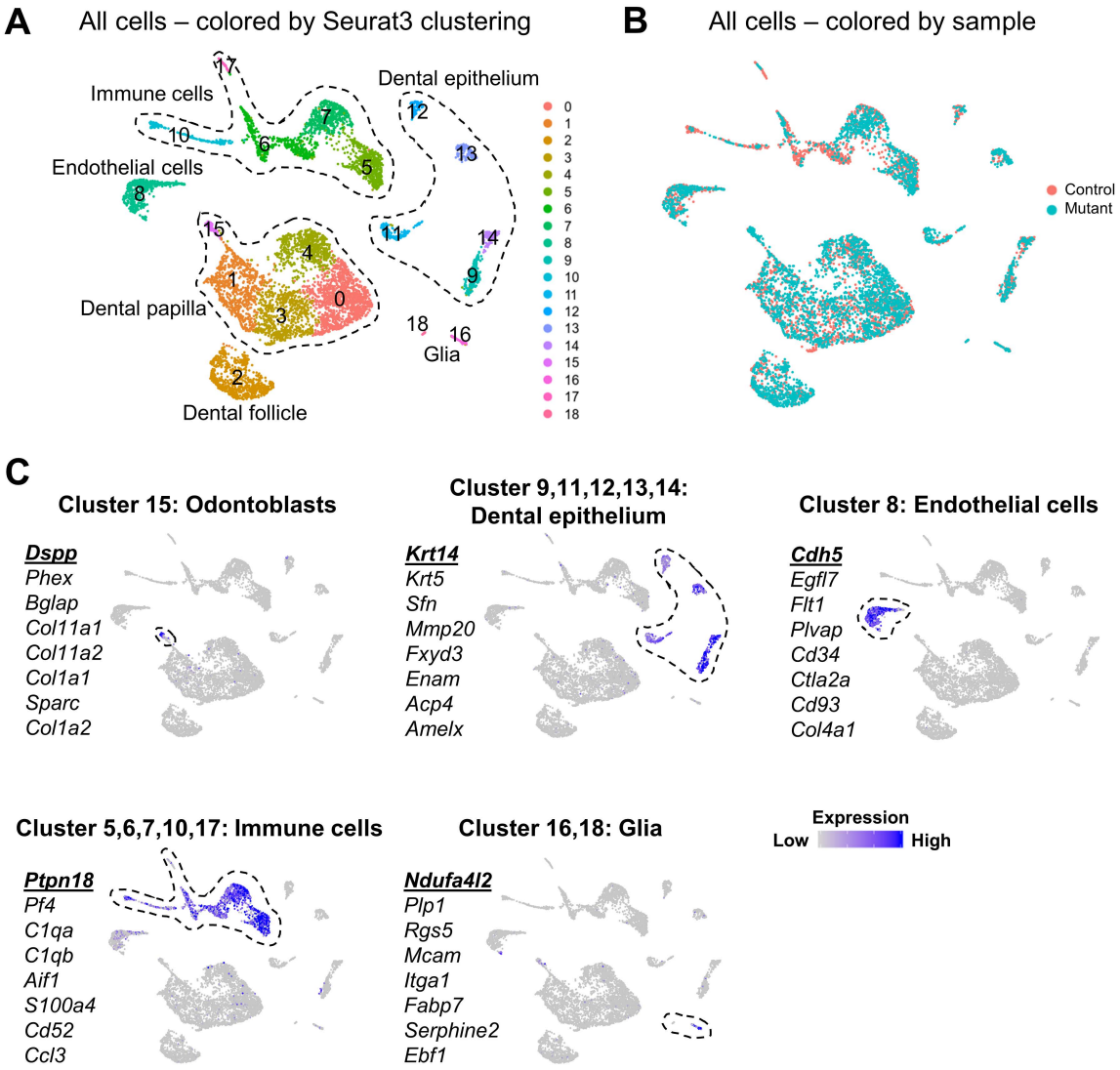
A
All cells – colored by Seurat3 clustering
Immune cells
Dental epithelium
Endothelial cells
Dental papilla
Glia
Dental follicle
0
1
2
3
4
5
6
7
8
9
10
11
12
13
14
15
16
17
18
B
All cells – colored by sample
Control
Mutant
C
Cluster 15: Odontoblasts
Dspp
Phex
Bglap
Col11a1
Col11a2
Col1a1
Sparc
Col1a2
Cluster 9,11,12,13,14:
Dental epithelium
Krt14
Krt5
Sfn
Mmp20
Fxyd3
Enam
Acp4
Amelx
Cluster 8: Endothelial cells
Cdh5
Egfl7
Flt1
Plvap
Cd34
Ctla2a
Cd93
Col4a1
Cluster 5,6,7,10,17: Immune cells
Ptpn18
Pf4
C1qa
C1qb
Aif1
S100a4
Cd52
Ccl3
Cluster 16,18: Glia
Ndufa4l2
Plp1
Rgs5
Mcam
Itga1
Fabp7
Serphine2
Ebf1
Expression
Low
High

S-Figure 6

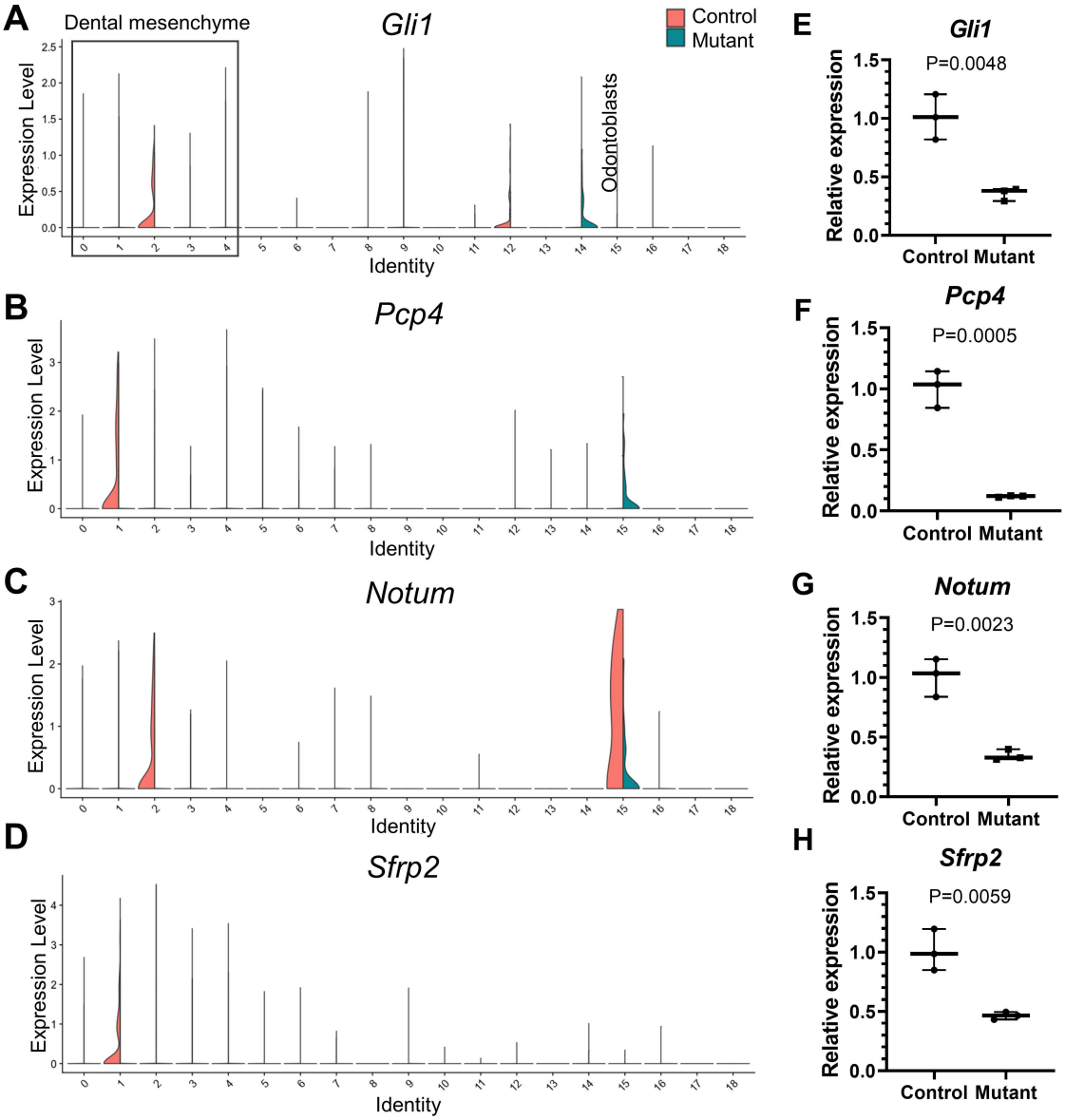
A
Dental mesenchyme
Gli1
Control
Mutant
Odontoblasts
Expression Level
Identity
B
Pcp4
C
Notum
D
Sfrp2
E
Gli1
P=0.0048
F
Pcp4
P=0.0005
G
Notum
P=0.0023
H
Sfrp2
P=0.0059
Relative expression
Control Mutant

S-Figure 7

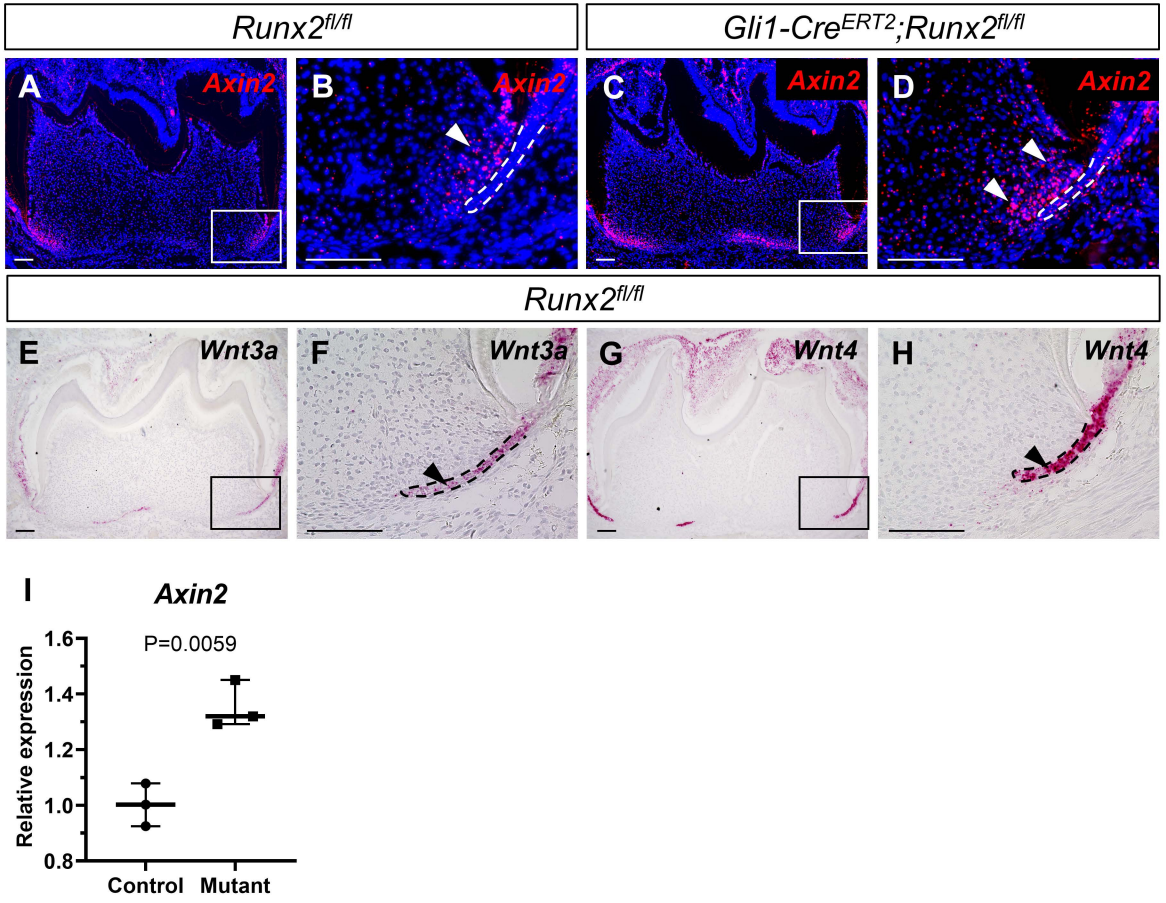
Runx2fl/fl
Gli1-CreERT2;Runx2fl/fl
A
Axin2
B
Axin2
C
Axin2
D
Axin2
Runx2fl/fl
E
Wnt3a
F
Wnt3a
G
Wnt4
H
Wnt4
I
Axin2
P=0.0059
Relative expression
1.6
1.4
1.2
1.0
0.8
Control
Mutant

S-Figure 8

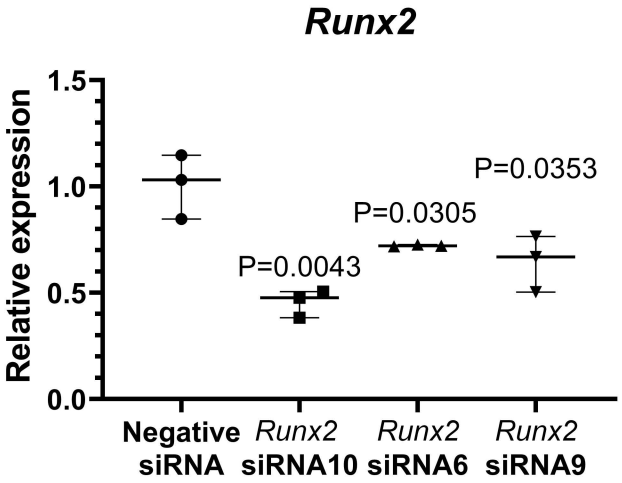

S-Figure 9

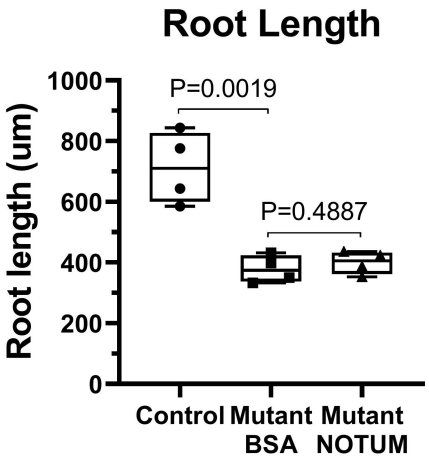

Supplemental Table 1. Primer List

Gapdh	Forward Primer: AGGTCGGTGTGAACGGATTTG Reverse Primer: TGTAGACCATGTAGTTGAGGTCA
Dspp	Forward Primer: ATTCCGGTTCCCCAGTTAGTA Reverse Primer: CTGTTGCTAGTGGTGCTGTT
Gli1	Forward Primer: GCCACCAAGCCAACTTTATG Reverse Primer: GAGAGTTGATGAAAGCCACC
Pcp4	Forward Primer: GACCAACGGAAAAGACAAGAC Reverse Primer: CAAGGAAAATAGTTGCAGAGG
Sfrp2	Forward Primer: CGTGGGCTCTTCCTCTTCG Reverse Primer: ATGTTCTGGTACTCGATGCCG
Notum	Forward Primer: GGACAGCTTTATGGCGCAAG Reverse Primer: TCACCGACGTGTTCAGCAG
Runx2	Forward Primer: GACTGTGGTTACCGTCATGGC Reverse Primer: ACTTGGTTTTTCATAACAGCGGA